membranes

MDPI

Review

Two-Dimensional Membranes for High-Value Ion Separation from Seawater and Brines

Wenjuan Zhang [1,†], Yue Yu [1,†], Ningning Liu [1,*], Zhiwei Wang [2] and Jianran Ren [3]

[1] Tianjin Key Laboratory of Aquatic Science and Technology, School of Environmental and Municipal Engineering, Tianjin Chengjian University, Tianjin 300384, China
[2] Tianjin Municipal Engineering Design & Research Institute Co., Ltd., Tianjin 300392, China
[3] China Southwest Architecture Design and Research Institute Co., Ltd., No. 8 Xinghui West Road, Chengdu 610041, China
* Correspondence: nnliu@tcu.edu.cn
† These authors contributed equally to this work.

Abstract

Seawater and brines contain substantial inventories of high-value ions, yet their extraction is constrained by dilute targets, concentrated competitors and feed-dependent speciation. Two-dimensional (2D) membranes offer short, tunable pathways that can amplify subtle differences in ion size, hydration, charge, and coordination. This review integrates ionic properties and aqueous speciation with membrane structure to establish a mechanistic framework for ion selectivity in 2D nanochannels. It critically examines size exclusion, dehydration, electrostatic partitioning, chemical recognition, and coupled non-ideal transport and evaluates their relevance to Li, U, Cs, Sr, Rb, and other underexplored ions. Major membrane platforms, including graphene-based materials, MXenes, transition-metal dichalcogenides, 2D metal–organic and covalent organic frameworks, layered inorganic materials and heterolamellar composites, are compared in terms of channel architecture, chemical tunability, stability, and manufacturability. The available evidence indicates that selectivity is not an intrinsic property of a nominal pore or material class, but an operating-state response of the coupled ion–solvent–membrane–electrolyte system. Finally, this review critically examines rational membrane-design strategies, outstanding challenges and future research priorities to guide the development of high-performance 2D membranes for the selective separation of high-value ions.

Keywords: two-dimensional membranes; high-value ions; selective separation; nanoconfinement; chemical recognition

Check for updates

Academic Editors: Francesca Macedonio and Sanghyun Jeong

Received: 10 September 2026
Revised: 9 October 2026
Accepted: 22 October 2026
Published: 30 October 2026

Copyright: © 2026 by the authors. Licensee MDPI, Basel, Switzerland. This article is an open access article distributed under the terms and conditions of the Creative Commons Attribution (CC BY) license.

1. Introduction

The transition towards electrified transport, low-carbon energy systems and advanced manufacturing is increasing demand for strategic metals, including lithium (Li), uranium (U), caesium (Cs), rubidium (Rb) and other rare earth elements (REEs), yet terrestrial reserves of these minerals suffer from depletion, severe mining pollution and geopolitically monopolized supply chains [1–3].

As a uniformly distributed liquid mineral reservoir across the globe, seawater serves as a viable substitute for dwindling terrestrial metal deposits. The dissolved lithium reserve in seawater totals 2.31×10^{11} tonnes, and its uranium resources amount to 4.5×10^{9} tonnes [4]. The oceanic uranium inventory is about 260 times larger than the conventional terrestrial uranium resources reported in the corresponding assessment [5].

Relevant estimates demonstrate that extracting target metals from merely 0.1% of global seawater can satisfy worldwide lithium and magnesium demand for over 50,000 years, which fundamentally mitigates the long-term supply shortage of land-based strategic minerals [6]. Compared with open seawater, natural and anthropogenic brines constitute more concentrated and geographically localized reservoirs of high-value ions. Lithium concentrations of approximately 40–3020 mg L^{-1} have been reported in salt lake brines, whereas geothermal brines commonly contain approximately 25–1000 mg L^{-1} lithium [7]. In addition to lithium, brines may contain considerable quantities of magnesium, potassium, calcium, bromine, strontium, rubidium, caesium, boron and uranium, depending on their geological origin and degree of evaporation [7].

The selective recovery of target ions from seawater and brines is inherently challenging, as the physicochemical disparities between a given ion and its principal interferents are often marginal relative to the marked compositional imbalance of the feed. Li^+ must be separated from Mg^{2+}, Na^+ and K^+; Rb^+ competes with K^+ and Cs^+; and uranium in carbonate-bearing seawater exists as negatively charged or neutral complexes, not as a bare cation. Consequently, selectivity values from binary solutions vary with pH, ionic strength, counterions and competing species, which alter hydration, charge screening or speciation.

Traditional separation routes, including adsorption, ion exchange, solvent extraction, precipitation, and electrochemical methods, have long been investigated to reclaim valuable dissolved ions from seawater and salt lake brine. Nevertheless, all these conventional techniques suffer from prominent drawbacks when applied to high-salinity marine water, such as weak ion discrimination and unsatisfactory environmental sustainability [8]. Among currently feasible techniques, membrane separation, such as nanofiltration (NF), offers robust, low-energy and pollution-free pathways for targeted ion migration. Serving as semipermeable interlayers, these membranes enable the penetration of target components while rejecting interfering substances, thereby achieving differentiated ion permeation performance [9,10]. The fabrication of high-performance separation membranes demands appropriate raw material selection paired with rational design of internal nanochannel architectures. On the one hand, candidate substrates must possess outstanding chemical inertness and thermal stability to withstand prolonged operation in harsh high-salinity marine environments. On the other hand, the finished membranes require an ultrathin framework embedded with abundant, tunable nano/sub-nanopores. A thinner membrane matrix minimizes mass-transfer resistance and elevates water flux, whereas narrowly sized, surface-functionalized channels are essential to discriminate ions based on disparities in hydrated radius and chemical affinity, thereby balancing permeability and ion selectivity simultaneously [11].

Two-dimensional materials offer an unusual degree of structural and chemical control over ion-transport pathways. Representative building blocks include graphene, graphene oxide (GO), reduced GO, MXenes, transition-metal dichalcogenides, hexagonal boron nitride, layered clays, two-dimensional covalent organic frameworks (COFs) and metal–organic frameworks (MOFs) [12]. Their atomic-scale thickness can shorten transport distances, while their surfaces provide sites for charge regulation, crosslinking, and molecular recognition. These properties create opportunities to couple rapid transport with ion-specific energy barriers [9,10,13–15]. Benefiting from these advances, 2D membranes have achieved rapid development in recent years (Figure 1A). The keyword network reveals a highly interconnected research landscape centred on graphene oxide (Figure 1B). This research base encompasses lamellar transport, interlayer-spacing control, nanofiltration and desalination, alongside communities associated with molecular simulation, ion transport, MOF/COF membranes, MXene-enabled water treatment and chiral separation. The temporal overlay

indicates comparatively recent activity around MXene, framework membranes and selected ion-separation concepts (Figure 1C).

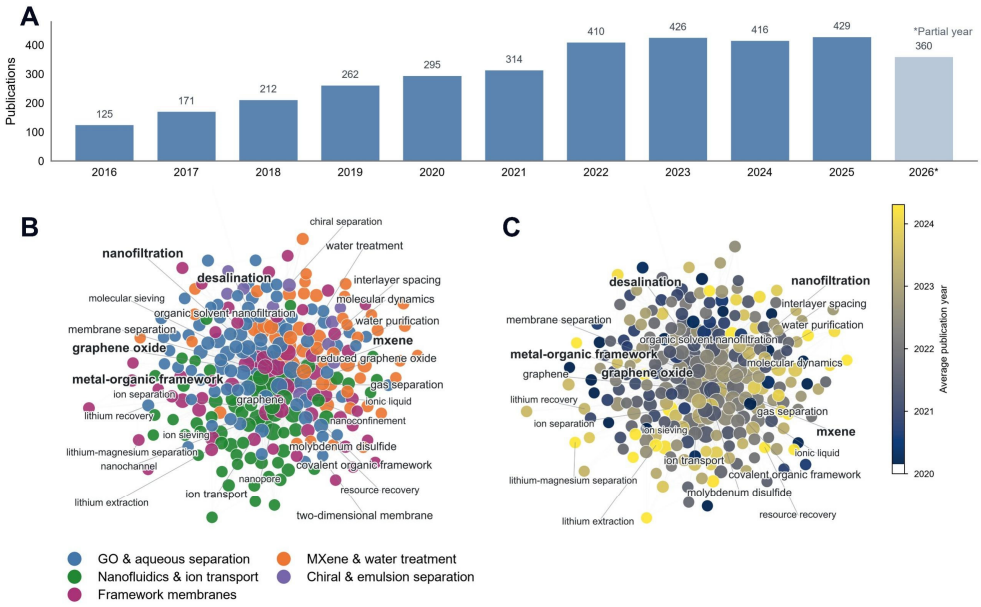


Figure 1. Bibliometric landscape and evolution of research on two-dimensional membranes for separation. Data were retrieved from the Web of Science Core Collection, with search completed in June 2026. (**A**) Annual publication counts from 2016 to 2026 (2026* represents partial-year publications up to June). (**B**) Author-keyword co-occurrence network for keywords. (**C**) Temporal overlay using identical nodes, edges, sizes and coordinates.

Based on the structural configuration and dominant transport pathways, 2D nanofiltration membranes can be broadly divided into two fundamental architectures: single-layer porous nanosheet membranes (Figure 2A) and restacked laminar membranes (Figure 2B). Single-layer membranes rely on intrinsic, artificially generated or defect-derived in-plane pores. Their atomically short transport length minimizes hydraulic resistance and offers high permeance potential. However, experimentally observed separation performance is highly sensitive to the pore-size distribution, chemical termination of pore edges, mechanical integrity of the suspended nanosheet and defect-free sealing between the selective layer and its support. Restacked laminar membranes form interconnected slit-shaped galleries between adjacent nanosheets. Such membranes are generally more amenable to solution-based processing and large-area fabrication, while their extended transport pathways provide greater opportunities for size exclusion, electrostatic interactions and chemical recognition. Nevertheless, ion transport through these membranes is strongly affected by aqueous swelling, channel tortuosity, stacking disorder and non-selective pathways associated with sheet edges or framework defects. Importantly, the XRD-derived d-spacing represents the basal-plane distance and is not equivalent to the free width accessible to water and ions. The geometric gallery height can be approximated as $h_{geom} = d_{wet} - t_{sheet}$, where d_{wet} is the hydrated basal spacing and t_{sheet} is the material-specific nanosheet thickness. For GO laminates, subtracting an approximate sheet thickness of 3.4 Å converts a dry d-spacing of 7.6–8.0 Å into a nominal gallery height of 4.2–4.6 Å, whereas hydration to 13–14 Å increases it to approximately 9.6–10.6 Å [16]. Surface functional groups, adsorbed ions and structured confined water occupy part of the nominal gallery volume, making the effective transport aperture smaller than the geometric spacing inferred from XRD. Hydrated-state or operando characterization under representative feed conditions therefore provides a more physically relevant basis for interpreting ion-sieving behaviour than dry-state XRD [17].

Porous framework and hybrid membranes constitute a practically important extension of these architectures (Figure 2C). In these systems, transport may occur simultaneously through intrinsic MOF or COF pores, intercrystalline boundaries and lamellar galleries. Their performance consequently depends not only on the properties of individual pores but also on the connectivity and relative contributions of multiple transport pathways.

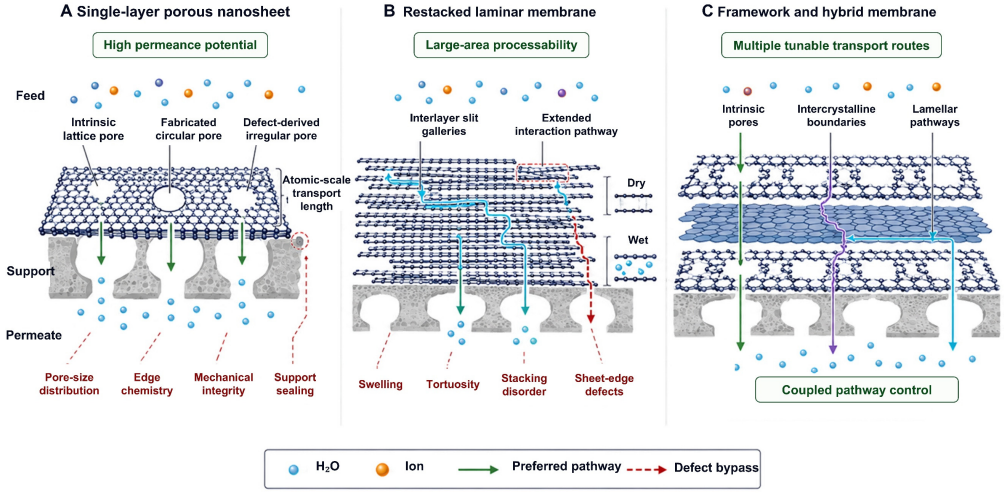


Figure 2. Schematic illustration of fundamental structural configurations for two-dimensional nanofiltration membranes.

The central opportunity offered by 2D membranes is the integration of channel geometry with channel chemistry. Interlayer spacing can be adjusted through ionic intercalation, molecular pillars, covalent crosslinking and water-content control [16,18]. Surface charge can be modified through protonation, terminal-group engineering and polyelectrolyte deposition [19,20]. Crown ethers, oligoethers, ion-exchange phases, peptides and other recognition groups can differentiate ions that cannot be resolved through size or valence alone [21,22]. Hybridization can further separate mechanical and chemical functions by using one component to stabilize the structure and another to recognize or conduct the target. These features position 2D membranes between conventional nanofiltration and affinity-based separation. They can act as pressure-driven selective layers, ion-conducting barriers, electrodialysis components or supports for reversible binding sites. This flexibility is especially valuable for resource recovery, where a single membrane may not provide the complete conversion from dilute feed to isolated product.

This review develops a mechanistically grounded framework for designing 2D membranes for the selective extraction of high-value ions from seawater and brines. It relates ionic size, hydration, valence, polarizability, and aqueous speciation to the free-energy landscape governing partitioning and transport within confined channels. The individual and coupled contributions of size exclusion, dehydration, electrostatic partitioning, chemical affinity and non-ideal transport are critically assessed. Evidence concerning Li, U, Cs, Sr, Rb, and less-explored ions is synthesized to identify target-specific separation requirements and disparities in research maturity. Major 2D membrane platforms are compared in terms of channel architecture, chemical tunability, wet-state stability, defect susceptibility, and manufacturability. This integrated analysis delineates the conditions governing ion selectivity, exposes critical evidence gaps and identifies priorities for developing stable, predictable and scalable high-value ion-selective membranes. It should be noted that while ocean-derived seawater and salt lake brines serve as the primary performance benchmark in this review, relevant mechanistic insights are also drawn from studies of acidic nuclear wastewaters. Many nanochannel transport phenomena, dehydration barriers and ion-sieving rules exhibit

strong technical overlaps across these feed systems, even though the feed ionic strength, pH and dominant ion species differ substantially. When interpreting reported separation performance, readers are reminded to distinguish results obtained from synthetic single-salt solutions, artificial seawater, and authentic complex brine matrices.

2. Ion Selectivity Mechanisms in 2D Membranes

Ion transport through 2D membranes arises from the coupling among ionic properties, solution chemistry and membrane structure under operating conditions. Size exclusion, dehydration, electrostatic interactions and chemical recognition are often treated as distinct mechanisms (Figure 3), yet each contributes to a common free-energy landscape. During permeation, an ion partitions from the bulk solution into the membrane entrance, reorganizes its hydration shell, traverses the confined pathway and ultimately desorbs into the receiving phase. The energetic cost of each stage depends on channel dimensions, surface chemistry, local water structure, competing ions and the imposed driving force. Ion selectivity is best understood as a state-dependent property of the complete ion–water–membrane system.

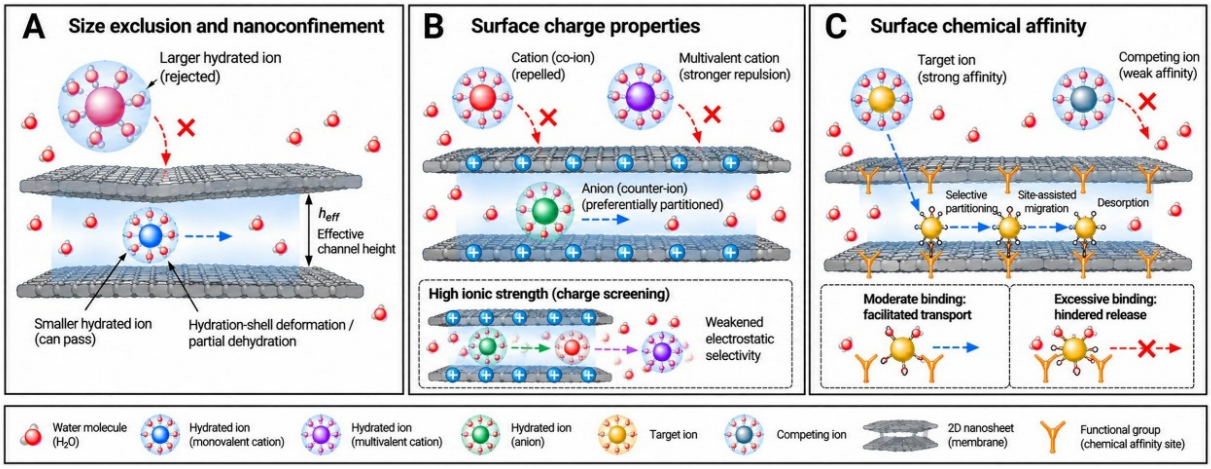


Figure 3. Principal mechanisms of selective ion transport in two-dimensional nanosheet membranes.

2.1. Ionic Properties and Speciation

Ion selectivity arises from differences in the thermodynamic penalty of entering a membrane channel and the kinetic resistance to migration within it. Ion permeability can be described through two coupled contributions: partitioning between the feed and membrane phases, and mobility along the transport pathway. Ionic charge, size and chemical affinity provide useful initial descriptors [22].

In aqueous media, hydration transforms bare ionic size into an effective transport scale. Bare-ion radii are reported as Shannon effective ionic radii for sixfold coordination. Effective hydrated radii are based on the Nightingale hydration-radius scale (Table 1). Small ions with high charge density, particularly Li^+ and Mg^{2+}, interact strongly with surrounding water and may exhibit larger hydrated radii than heavier monovalent ions. Consequently, the size sequence relevant to confined transport can differ substantially from that inferred from crystallographic radii. Moreover, hydrated radius is not a uniquely defined molecular dimension. Values derived from ionic mobility, structural measurements or solvation models can differ because they describe distinct aspects of the hydration environment [23]. Recent experiments and simulations further demonstrate that hydration shells are distorted, reorganized or partially removed when ions enter angstrom-scale pores and two-dimensional nanoslit [24].

Valence introduces additional effects through hydration energy, ion pairing, electrostatic partitioning and interactions with membrane functional groups. For example, Li^+ and Mg^{2+} possess comparable crystallographic radii but markedly different hydrated dimensions and dehydration penalties. Their separation cannot be interpreted using bare size alone. In contrast, Rb^+ and Cs^+ have different bare radii but nearly identical Nightingale hydrated radii, indicating that size-based discrimination between them may be intrinsically limited. Because counterions maintain electroneutrality, ionic fluxes are also coupled. Measured permeation consequently reflects the collective transport of ions and salts rather than the motion of isolated point charges [24,25].

Hydration-based comparisons remain incomplete because pH, ionic strength and ligand composition determine the chemical species presented to the membrane. Hydrolysis, carbonate or sulfate complexation, and ion pairing can alter ionic charge, geometry and membrane affinity. In seawater, U(VI) is predominantly associated with calcium–uranyl–carbonate complexes [26]. Multicomponent feeds additionally introduce competition for channel volume, charged sites and coordination groups. Ion selectivity should be interpreted as an operating-state property of the coupled ion–solvent–membrane–feed system.

Table 1. Bare-ion and effective hydrated radii of representative ions.

Ion or Species	Bare-Ion Radius (Å)	Effective Hydrated Radius (Å)	Reference
Li^+	0.76	3.82	[22]
Na^+	1.02	3.58	[27]
K^+	1.38	3.31	[28]
Rb^+	1.52	3.29	[28]
Cs^+	1.67	3.29	[25]
Mg^{2+}	0.72	4.28	[24]
Ca^{2+}	1.00	4.12	[24]
Sr^{2+}	1.18	4.12	[23]

2.2. Size Sieving and Nanoconfinement

Size sieving provides the geometric basis for ion discrimination in 2D membranes. In atomically thin membranes, selectivity is governed primarily by the effective diameter and size distribution of in-plane pores. In restacked lamellar membranes, transport occurs through interconnected slit-shaped galleries, whose accessible height is determined by nanosheet stacking and surface structure [29,30].

Given that ions are presented to these confined channels as hydrated entities rather than as naked ions in aqueous solutions, three approximate transport regimes can be identified: (1) channels substantially larger than the hydrated ion provide limited size discrimination; (2) channels approaching the hydrated dimension impose strong steric partitioning and hydration-shell deformation; (3) ions are effectively excluded when the free aperture is smaller than the minimum cross-section attainable without an energetically prohibitive loss of hydration water. Hydrated radius should nonetheless be regarded as a relative descriptor, not as a fixed sieving criterion. Under angstrom-scale confinement, hydration shells may deform, partially dehydrate or reorganize with the confined water structure, thereby altering both ion partitioning and mobility.

Effective size sieving consequently requires angstrom-level control over both the mean aperture and its distribution. Chen et al. [16] demonstrated that K^+, Na^+, Ca^{2+}, Li^+ and Mg^{2+} could regulate the interlayer spacing of graphene oxide membranes with angstrom precision. Membranes conditioned by one cation subsequently excluded ions requiring larger hydrated volumes. However, first-principles calculations attributed the structural

regulation to preferential cation adsorption at regions containing both oxide groups and aromatic domains. This result indicates that the observed sieving arose from chemically regulated confinement rather than geometry alone. In atomically thin graphene, Zhao et al. [22] similarly produced pores predominantly within the range of 3.5–8.5 Å and observed near-complete blockage of ions with hydrated diameters above approximately 9 Å. Their results also showed that partial dehydration contributed to the transport barrier when pore dimensions approached the hydration scale.

Maintaining such dimensional precision in water remains a central challenge for lamellar membranes. Molecular crosslinking, ion intercalation and rigid nanopillars can suppress swelling and stabilize the transport galleries, but these modifications may also alter surface charge, affinity and tortuosity. For example, Zhang et al. [31] used cetyltrimethylammonium chloride intercalation to tune montmorillonite channel heights between 0.40 and 0.52 nm. Decreasing the channel height from 0.504 to 0.440 nm increased the reported Na^+/Cs^+ separation factor from 190.99 to 1039.79. Nevertheless, this performance should not be attributed exclusively to hard-sphere sieving because interlayer ion exchange and surfactant–ion interactions may also contribute. Size selectivity is most reliable when the wet-state aperture is narrowly distributed and stable, while chemical interactions remain sufficiently characterized to distinguish geometric exclusion from coupled transport effects. It is worth emphasising that non-covalent coordination and cation-π interactions, which stabilize tuned interlayer spacing, may degrade if feed concentration ratios shift significantly during long-term operation. Large variations in competing cation abundance can alter the ion-intercalation equilibrium, resulting in a drift in the real-world working aperture even if material chemistry remains unchanged.

2.3. Surface Charge Properties

Surface charge regulates ion partitioning at membrane entrances and within confined nanochannels, thereby complementing size-based discrimination. Charge may originate from ionizable functional groups, lattice substitutions, exposed edges or adsorbed modifiers. GO, MXene and functionalized MoS_2 membranes exhibit charge states that depend on both material composition and solution conditions. Because protonation and ion adsorption vary with pH and electrolyte composition, surface charge is an operating-state property rather than an invariant material parameter.

Fixed charges generate an electrostatic potential difference between the membrane phase and the bulk solution. Counterions are preferentially partitioned into charged channels, whereas co-ions experience an energetic penalty at the membrane–solution interface. This Donnan-type exclusion is generally stronger for multivalent co-ions. However, salt transport remains constrained by electroneutrality, meaning that electrostatic attraction of one ion does not necessarily result in unrestricted salt permeation. The accompanying counterion and co-ion fluxes must be considered together.

Surface-charge engineering provides an effective means of regulating mono-/divalent-ion separation. Polyelectrolyte modification of GO membranes has produced high rejection of multivalent salts while retaining substantial water permeance. Similarly, positively charged PEI-modified GO/MXene membranes combined Donnan exclusion with confined transport, resulting in substantially higher rejection of Mg^{2+} than Li^+ [32]. PDDA-modified MXene membranes also exhibited improved Li^+/Mg^{2+} selectivity following the introduction of positive charge [33]. These results demonstrate that charge regulation is particularly useful when competing ions have similar dimensions but different valences.

Nevertheless, electrostatic selectivity depends strongly on channel dimensions and feed concentration, and the Donnan-exclusion rules established in dilute systems cannot be extrapolated directly to real seawater or brines. Electric-double-layer overlap can dominate

transport in narrow channels at low ionic strength, whereas the high ionic strength of concentrated seawater and brines gives rise to intense charge screening that compresses the electric double layer, diminishes the electrostatic potential difference across the membrane–solution interface and substantially attenuates Donnan exclusion. Specific ion adsorption may additionally neutralize or reverse the effective channel charge. Measurements obtained in dilute single-salt solutions may therefore markedly overestimate charge-based selectivity under realistic conditions, so direct extrapolation from low-concentration electrostatic regimes to high-salinity feeds should be avoided. Mechanistic interpretation should combine pH-dependent transport, concentration-dependent measurements and surface-charge characterization in relevant electrolytes.

2.4. Surface Chemical Affinity

Surface chemical affinity provides ion-specific discrimination beyond general size and charge effects. Functional groups within 2D nanochannels can coordinate permeating ions, replace hydration water or stabilize intermediate transport states. This mechanism is particularly important for ions with similar charge and hydrated dimensions, for which steric exclusion and Donnan partitioning alone provide limited selectivity [30,34,35].

Affinity influences both membrane partitioning and intrachannel mobility. Moderate ion–site interactions may compensate for dehydration penalties and promote ion entry [36]. By contrast, excessively strong binding can create deep free-energy minima, increase residence time and hinder ion release [37]. A high adsorption capacity does not necessarily correspond to high permeability. Effective recognition sites must balance selective partitioning, site-to-site migration and desorption into the receiving phase.

Crown ethers provide a representative strategy for incorporating size-matched coordination sites into 2D nanochannels. Crown ether-confined MXene membranes have achieved reported Li^+/Mg^{2+} and K^+/Mg^{2+} selectivities of 39 and 40.2, respectively [38]. However, the observed performance may arise from the combined effects of cavity recognition, channel-size modification and altered charge distribution. These contributions should be distinguished before attributing selectivity solely to host–guest complexation. EDTA-functionalized MXene membranes further illustrate the coupling between chemical recognition and nanoconfinement. Anchored EDTA groups preferentially interact with multivalent cations, while their protonation state regulates local charge density [20]. Experimental and computational evidence indicates that ion recognition, partial dehydration and electrostatic interactions jointly determine membrane entry and migration. Similarly, polyacrylic acid-functionalized GO membranes exhibit chemically gated transport because ion binding changes polymer conformation and the local channel environment [13].

Chemical affinity can further be tailored through amine, carboxylate, sulfonate and phosphate groups, as well as biomimetic coordination motifs [37]. The appropriate ligand depends on the target species present under actual feed conditions. Uranium recovery, for example, requires recognition of uranyl–carbonate species rather than free UO_2^{2+} in seawater [39]. Ligand selection must account for pH-dependent speciation, competitive binding and the concentration excess of major seawater ions.

Affinity-based separation remains sensitive to site saturation, irreversible complexation and competitive occupation. Functional groups may also undergo protonation changes, leaching or chemical degradation during repeated operation. Consequently, affinity-based membranes should be evaluated using multicomponent feeds and repeated adsorption–desorption or permeation–regeneration cycles. Such evidence is necessary to distinguish reversible ion recognition from nonspecific accumulation or progressive membrane blockage.

2.5. Computational Approaches for Elucidating Ion Selectivity

Computational methods provide complementary descriptions of ion transport across electronic, molecular and membrane scales. Density functional theory (DFT) resolves local coordination and charge transfer, whereas molecular dynamics (MD) describes hydration and migration. Continuum models further connect these molecular processes with macroscopic concentration and potential fields. Their mechanistic value depends on whether calculated descriptors can be related to experimentally measurable partitioning, mobility and permeability.

DFT is principally used to examine local interactions between ions and chemically heterogeneous nanochannels. Adsorption energies, charge-density differences and electrostatic-potential maps can identify preferred coordination sites and distinguish ion-specific recognition from nonspecific electrostatic attraction [40]. Zhang et al. compared the electrostatic-potential distributions of fully and partially deprotonated two-dimensional polyimine membranes (Figure 4A) [41]. The binding-energy calculations showed that hydrated Na^+ interacted more strongly with the membrane than hydrated K^+ across the examined hydration states, indicating that membrane protonation controls both the spatial distribution and strength of ion-coordination sites. Similar calculations for functionalized covalent organic framework (COF) membranes distinguish direct Na^+ or K^+ coordination from water-mediated Li^+ association [42,43]. These studies demonstrate that binding energy describes local affinity but cannot independently predict permeability. Stronger binding may promote membrane entry, yet excessive stabilization can impede intrachannel migration and ion release.

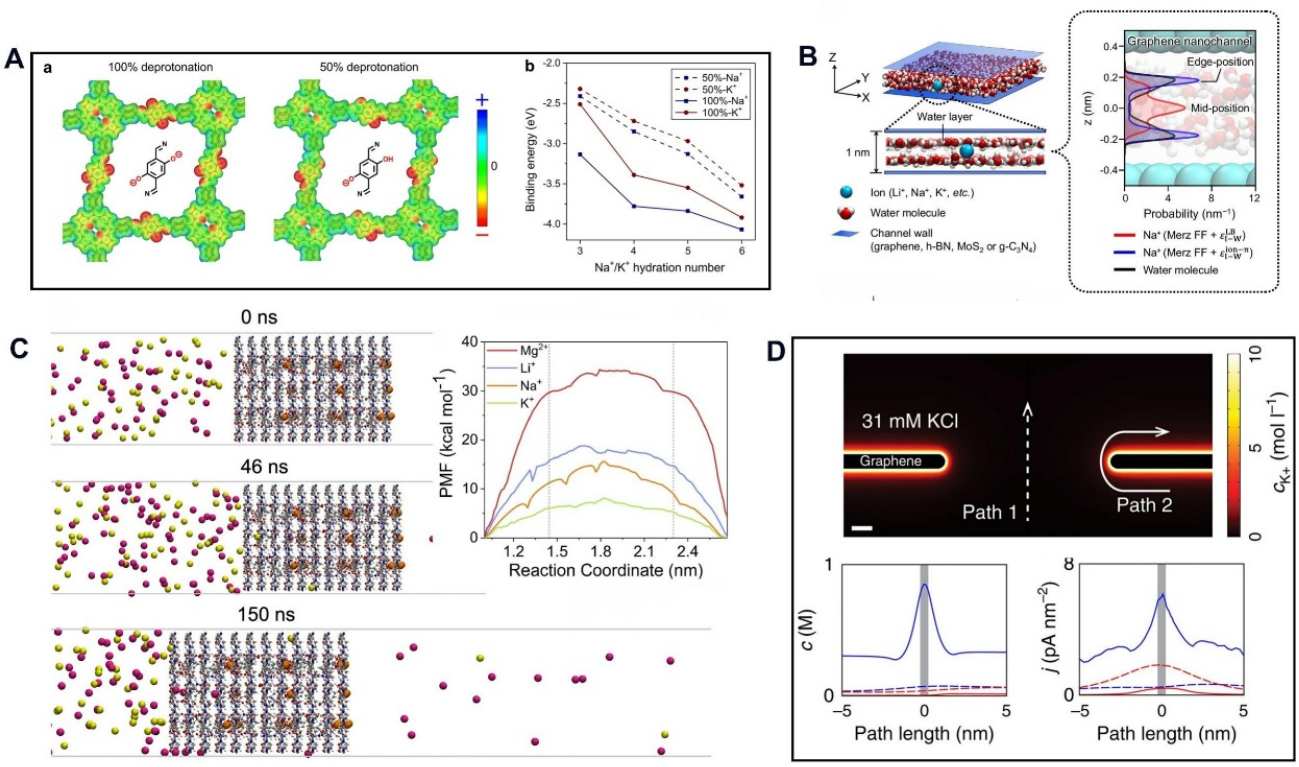


Figure 4. (**A**) a: Electrostatic–potential distributions and b: ion–binding energies calculated for fully and partially deprotonated 2D polyimine membranes. Reprinted from [41]. (**B**) Spatial distributions of first–shell water molecules around Li^+, Na^+ and K^+ at different positions in a graphene nanochannel. Reprinted from [28]. (**C**) Simulated transmembrane trajectories and PMF profiles for K^+, Na^+, Li^+ and Mg^{2+} transport through a MOF–in–COF heterostructure channel. Reprinted from [44]. (**D**) PNP–calculated ion-concentration and current–density distributions in a graphene nanopore. Reprinted from [45].

Classical MD complements static DFT calculations by resolving the structural and temporal evolution of ions, water and membrane functional groups [46–48]. Radial distribution functions and coordination numbers quantify changes in ion hydration and ligand coordination between bulk solution and confined channels. Spatial density profiles identify preferential ion locations, whereas residence times, diffusion coefficients and transmembrane crossing events characterize mobility. Figure 4B presents the spatial distribution functions of first-shell water molecules around Li^+, Na^+ and K^+ at the middle and near-wall positions of a graphene nanochannel [28]. Li^+ and Na^+ retained approximately spherical hydration shells at the channel centre, whereas the K^+ hydration shell was divided into two ring-like water distributions. When the ions approached the channel wall, the hydration shells of all three ions became anisotropic and separated into ring- and pole-like regions. This result demonstrates that nanoconfinement alters the spatial organization of hydration water even when the nominal hydration number does not change substantially.

Nonequilibrium molecular dynamics (NEMD) extends these analyses by imposing an electric field, pressure gradient or chemical-potential difference to induce directional transport. The resulting ionic current can be decomposed into the intrapore carrier concentration and ion drift velocity. This distinction is important because preferential adsorption does not necessarily increase conduction. In few-layer MoS_2 nanopores, K^+ could occupy regions close to the pore wall, but these strongly adsorbed ions contributed little to the current [40]. Most of the conductive flux arose from ions separated from the wall by one or two water layers. The observed selectivity consequently reflected the combined effects of pore occupation, hydration-dependent mobility and confined-water dynamics rather than adsorption alone. Functional groups can also replace coordinating water and partially compensate for dehydration. Carbonyl groups, for example, may hinder Ca^{2+} entry into narrow graphene pores but stabilize partially dehydrated Ca^{2+} in wider pores [49].

Free-energy calculations provide a quantitative connection between molecular configurations and selective transport. Potentials of mean force (PMFs) are commonly obtained from classical MD using umbrella sampling, metadynamics or related enhanced-sampling methods. A one-dimensional PMF, $\Delta G\ (z)$, describes the free-energy change along a selected transmembrane coordinate. It can identify barriers and minima associated with ion entry, dehydration, intrachannel migration and release. Figure 4C combines MD snapshots with PMF profiles for K^+, Na^+, Li^+ and Mg^{2+} transport through a one-dimensional MOF-in-two-dimensional COF heterostructure channel [44]. The simulations showed that the transmembrane barriers followed the order K^+ (8.12 kcal mol^{-1}) < Na^+ (15.56 kcal mol^{-1}) < Li^+ (18.73 kcal mol^{-1}) < Mg^{2+} (34.51 kcal mol^{-1}). The substantially lower K^+ barrier agreed with its faster simulated permeation, attributing the simulated K^+ preference to the combined effects of pore-entrance sieving and relatively weak K^+–channel interactions, rather than to either factor alone. All reported potential-of-mean-force (PMF) energy barriers should be benchmarked against ambient thermal energy ($k_BT \approx 0.59$ kcal·mol^{-1} at 298 k) for comparative evaluation of transport resistance.

Continuum models extend the accessible length and time scales beyond those of atomistic simulations. Poisson–Boltzmann, Poisson–Nernst–Planck (PNP), Donnan–steric and finite-element models calculate ion concentration, electrostatic potential and species flux from channel geometry, membrane charge and applied driving forces [45]. Figure 4D shows a PNP model for a negatively charged graphene nanopore [45]. Profiles extracted through the pore centre and along the membrane surface further showed that the surface pathway contained a higher K^+ concentration and a markedly larger K^+ current density. Thus, the K^+/Cl^- selectivity was attributed to a highly conductive counterion pathway adjacent to the charged surface, rather than to steric exclusion by the pore alone.

Mechanistic inference is strongest when calculations at different scales are mutually constrained by experiments. DFT establishes local coordination energetics, while MD and free-energy methods determine their effects on partitioning and mobility. Continuum models assess whether molecular selectivity persists under concentration polarization, charge screening and membrane-scale gradients. Idealized, defect-free MD models must also be interpreted cautiously: by omitting pinholes, stacking disorder, swelling and chemical heterogeneity, they tend to overstate the resolving power of sub-nanometre channels and underestimate non-selective bypass flux. Force-field selection adds further uncertainty, because dehydration-energy barriers in sub-nanometre confinement are highly sensitive to ion–water and ion–channel interactions. Non-polarizable force fields, which treat ions and water as fixed point charges, neglect induced polarization and typically underestimate dehydration free energies and their associated barriers; polarizable force fields explicitly account for induced dipoles and charge redistribution, generally yielding higher, more ion-specific dehydration barriers closer to experimental hydration energetics, at the cost of greater computational expense and parametrization effort. Reported dehydration barriers from classical MD should therefore be viewed as force-field-dependent estimates, and quantitative comparisons are valid mainly within the same force-field family and water model. Future simulations should incorporate multicomponent electrolytes, wet-state pore-size distributions, swelling, chemical heterogeneity and non-selective defects.

2.6. Coupled and Non-Ideal Transport

The mechanisms described above rarely operate independently. For instance, narrowing a channel can simultaneously strengthen steric exclusion, increase dehydration barriers and enhance ion–surface interactions. Chemical functionalization also changes charge density, wet-state spacing and confined-water structure.

Wet-state structural evolution represents a major source of non-ideal behaviour in lamellar membranes. Water uptake can expand the interlayer galleries, broaden their dimensional distribution and reduce size-sieving precision. Conversely, strongly interacting multivalent ions may bridge adjacent nanosheets and restrict swelling. In situ microscopy and X-ray diffraction measurements of $Ti_3C_2T_x$ membranes have confirmed that intercalated-ion valence influences both water uptake and interlayer stability [37]. More recent work demonstrated that controlling the number of confined water layers through Cs^+ intercalation stabilized MXene nanochannels and modified Li^+/Mg^{2+} transport [50]. Consequently, dry-state spacing should not be construed as the operative pore dimension under hydrated operational conditions.

Structural defects create another discrepancy between ideal nanochannels and macroscopic membrane performance. Pinholes within nanosheets, intersheet voids, stacking disorder and imperfect membrane–support sealing can provide low-resistance bypass pathways. Even a small fraction of such pathways may dominate the measured flux and weaken apparent size selectivity. In GO membranes, non-ideal actinyl rejection has been attributed partly to pinhole defects, stacking voids and a nonuniform distribution of interlayer spacings [51]. Mechanistic studies should consequently report membrane thickness, effective area, structural uniformity and sample-to-sample variation rather than relying only on average X-ray diffraction spacings.

Feed-solution composition additionally modulates ion transport via electrostatic screening, ion pairing and competition for channel occupancy. Increasing ionic strength can weaken Donnan partitioning and reduce membrane permselectivity [51]. In functionalized MoS_2 channels, the cooperative transport observed at low concentration became substantially weaker at high salt concentration, indicating that screening and altered ion pairing changed the transport pathway [37]. Binary-mixture experiments with MXene

membranes similarly showed that strongly interacting cations preferentially occupied the interlayer galleries and reduced the selectivity predicted from separate single-salt measurements [52]. The magnitude and even direction of ion selectivity may depend on competitor concentration and the applied driving force.

These non-ideal effects establish an important boundary for mechanistic interpretation. Evidence obtained using dry membranes, dilute single-salt solutions or idealized defect-free models cannot be transferred directly to seawater and concentrated brines. Robust attribution requires wet-state structural characterization, multicomponent feeds, relevant ionic strength and extended operation. Selectivity should also be reported together with absolute flux, mass balance and membrane reproducibility. Such measurements are necessary to distinguish intrinsic nanochannel selectivity from transient sorption, defect-mediated transport and feed-dependent competition.

Under realistic continuous-flow conditions, the measured separation performance is governed not only by the intrinsic resistance of the nanochannels but also by concentration-polarization resistance, membrane and support-layer resistance and flow-dependent structural changes. Coupled mass-transfer models have demonstrated that the polarization layer can substantially influence the apparent rejection and permeate concentration in pressure-driven membrane processes [53]. For lamellar 2D membranes, applied pressure can further alter the channel dimensions and transport resistance through compaction or external confinement [54]. Moreover, cross-flow measurements at realistic solute concentrations have shown that membrane performance may differ substantially from that inferred from dilute or idealized laboratory tests [55]. Therefore, translation of nanochannel selectivity to continuous separation requires standardized reporting of membrane thickness, operating pressure, cross-flow velocity, feed composition and long-term performance.

3. Selective Separation and Recovery of Target Ions

High-value ions in seawater, salt lake brines and saline radioactive streams are important as alternative mineral resources and as targets for environmental remediation. Lithium supports rechargeable batteries and low-carbon energy systems, uranium is a key nuclear-fuel resource, and rubidium has strategic value in specialized technologies. Caesium and strontium are particularly significant in radioactive-water management, where their selective removal can reduce environmental risks. However, these ions occur at widely different concentrations and in different chemical forms and must be separated from abundant competitors with similar properties. This section reviews 2D membrane strategies for Li, U, Cs, Sr, Rb and other less-studied ions, linking their application importance and ion-specific separation challenges to reported performance and prospects for practical recovery.

3.1. Lithium Separation and Recovery

Lithium recovery from seawater is a trace-ion separation challenge because Li^+ occurs at concentrations far below those of Na^+, Mg^{2+}, Ca^{2+} and K^+. Salt lake brines generally contain more lithium but may exhibit high Mg/Li ratios, creating a different separation problem. Lithium-selective separation strategies using 2D membranes can be conceptually categorized into three major classes: (i) valency-based electrostatic discrimination, (ii) dehydration-driven size sieving and (iii) host–guest molecular recognition such as crown-ether coordination. This categorisation helps to decouple selectivity originating from charge differences (e.g., Li^+/Mg^{2+}) from same-valency discrimination (e.g., Li^+/Na^+, Li^+/K^+). Li^+/Mg^{2+} separation can exploit differences in valence, hydration and electrostatic partitioning. By contrast, Li^+/Na^+ and Li^+/K^+ separation requires discrimination among chemically similar monovalent ions. The small bare radius of Li^+ does not guarantee rapid transport because its strongly bound hydration shell imposes a substantial entry

barrier. Lithium selectivity depends on the coupled regulation of dehydration, resolvation, ion–channel interactions and confined diffusion.

Sub-nanometre confinement can amplify differences between Li^+ and its major competitors, but the channel chemistry must also support rapid transport. Poly(sodium 4-styrenesulfonate)-intercalated MXene membranes combined confined galleries with relatively weak Li^+–sulfonate interactions (Figure 5A) [56]. The reported Li^+ permeation rate reached 0.08 mol m^{-2} h^{-1}, with Li^+/Mg^{2+}, Li^+/Na^+ and Li^+/K^+ selectivities of 28, 15.5 and 12.7, respectively. Oligoether-functionalized covalent organic framework (COF) membranes provide a related example of solvation regulation (Figure 5B) [57]. Their Li^+/Mg^{2+} selectivity varied non-monotonically with oligoether-chain length because the same ligands affected both ion partitioning and intrachannel mobility. These results indicate that increasing ligand density or binding strength does not necessarily enhance selectivity. The optimal interaction should facilitate ion entry without creating a kinetically persistent adsorption state.

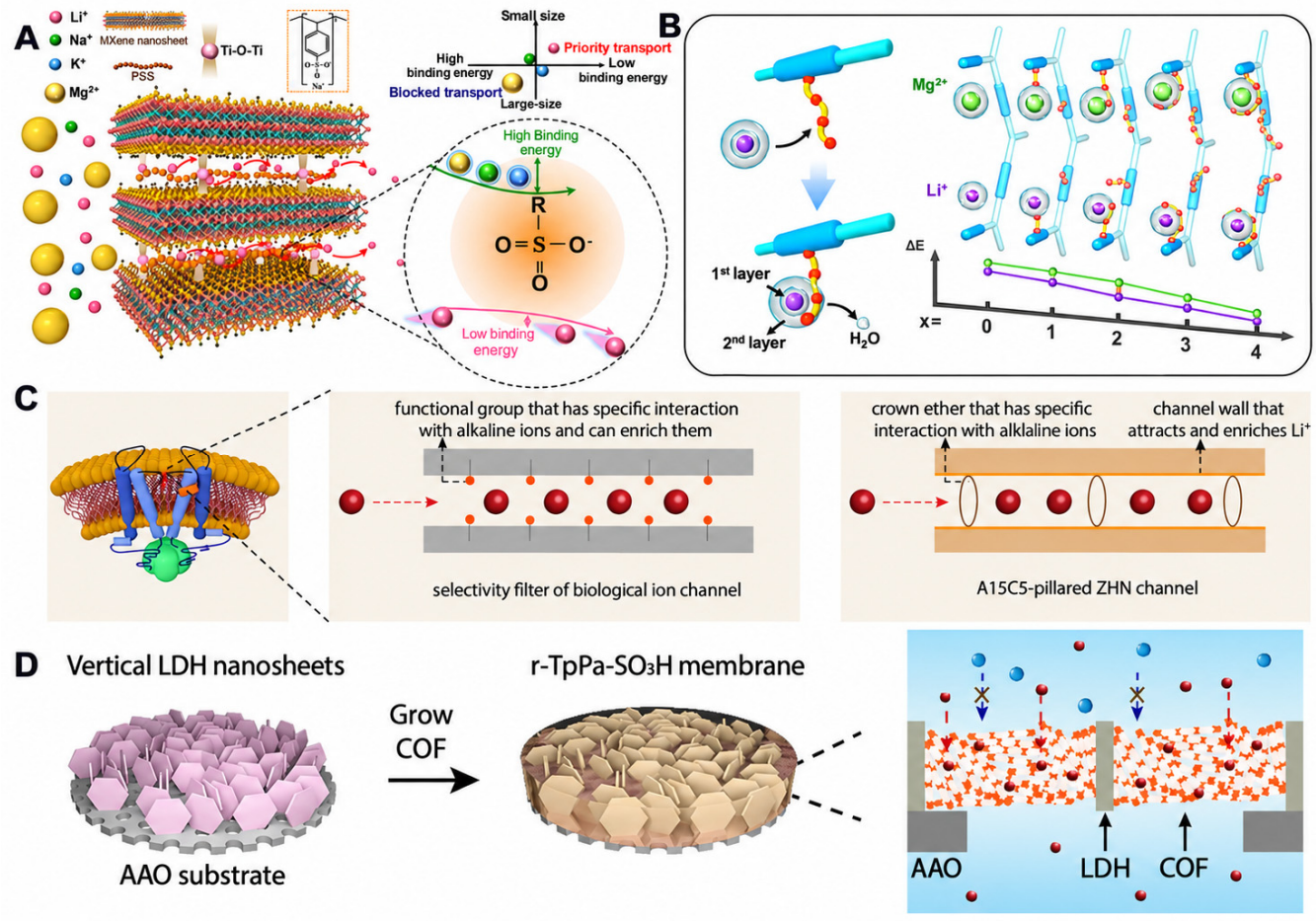


Figure 5. (**A**) Diagrammatic sketch of the fast transport subnanochannels for Li^+ in MXene/PSS composite membranes. Reprinted from [56]. (**B**) Conceptual diagram of engineering the solvation ability of COF membranes by tuning the length of oligoether chains. (**C**) Crown–ether–mediated recognition, confinement and local enrichment of trace Li^+ in A15C5–pillared ZHN channels. Reprinted from [58]. (**D**) Fabrication of the randomly oriented COF membrane. Reprinted from [42].

Electrostatic regulation is particularly relevant to Li^+/Mg^{2+} separation. Fixed charges alter interfacial ion partitioning and can impose higher entry barriers on divalent ions. For example, positively charged $Ti_3C_2T_x$ membranes reportedly achieved a Li^+/Mg^{2+} selectivity of 29.3 despite an interlayer spacing exceeding 2 nm, suggesting that electrostatic exclusion can partially compensate for channels that are too wide for strict size sieving. Nevertheless,

charge-mediated selectivity is not an invariant membrane property. Charge screening, ion–ion correlations and competitive channel occupation become increasingly important at high ionic strength, and the direction of selectivity may change with the applied voltage or concentration gradient. Water content is equally influential because confined water determines both channel dimensions and ion solvation. Modulating the water content of MXene laminates through cation intercalation reduced swelling and altered the population of transport defects, demonstrating that wet-state channel structure, rather than dry interlayer spacing, controls the operative ion pathway [50].

Discrimination between Li^+ and other alkali-metal ions generally requires more specific chemical interactions. Crown ether-pillared angstrom channels combine geometrical confinement, reversible Li^+ coordination and local ion enrichment (Figure 5C). In artificial seawater containing 25 μM Li^+, these channels produced a reported effective Li^+/Na^+ selectivity of 1422 [58]. It is critical to note that this high value was obtained under controlled artificial-feed conditions. It reflects enrichment performance under specific laboratory settings rather than steady-state continuous-flux permselectivity for authentic seawater; it may also partly originate from transient sorption enrichment effects. Direct extrapolation to real-world continuous recovery should be treated with caution. This result demonstrates the potential of molecular recognition at a seawater-relevant lithium concentration. However, it represents enrichment from a controlled artificial feed rather than continuous recovery from natural seawater. Heteropolyacid ligands incorporated into two-dimensional channels provide another recognition strategy by facilitating exchange between hydrated and ligand-coordinated states, producing a reported Li^+/K^+ permselectivity of 16 in a model system [59]. Collectively, these studies suggest that reversible and kinetically moderate coordination is preferable to maximally strong binding: insufficient affinity produces little discrimination, whereas excessive affinity converts a transport site into an adsorption trap.

Lithium enrichment can also be achieved by selectively transporting or immobilising competing ions rather than Li^+ itself. Crown ether-derived sites introduced into graphene oxide channels trapped Na^+ and improved Li^+/Na^+ discrimination [60]. This mechanism reflects Na^+ recognition rather than direct Li^+ recognition, but it demonstrates the potential of competitor-selective trapping. A randomly oriented sulfonated COF membrane employed a related but transport-based strategy (Figure 5D) [42]. Its confined pathways facilitated Na^+ and K^+ permeation while retaining Li^+. Under an appropriate electric field, Mg^{2+} and Ca^{2+} also permeated, producing a Li-rich retentate. The membrane was further evaluated using an actual Qinghai salt lake brine.

The molecular selectivity of a channel can only be expressed macroscopically when non-selective pathways are suppressed. Oversized pores, sheet-edge gaps, pinholes and swelling-induced defects may dominate the measured flux even when the nominal channel dimensions are within the angstrom range. Electrochemical repair of porous graphene membranes showed that masking oversized pores substantially improved Li^+/Mg^{2+} discrimination. Notably, the repair layer itself did not require specific Li^+ affinity [61]. Hybrid two-dimensional membranes further attempt to control channel geometry and chemistry simultaneously. Bimetallic metal–organic frameworks introduced into graphene oxide interlayers produced a reported Li^+/Mg^{2+} separation factor of 191 through combined size exclusion and transport-barrier regulation [62]. More recently, porous organic cages were converted into porous liquids and confined within graphene oxide laminates, reducing framework aggregation and interfacial defects. The resulting membrane exhibited a Li^+ permeance of 0.75 mol m^{-2} h^{-1} and a Li^+/Mg^{2+} selectivity of 154.4 in simulated brine, reversing an initial Mg/Li ratio of 40 to a Li/Mg ratio of 4.6 in the permeate [63]. Although this represents a substantial enrichment step, it does not yet establish downstream production of a purified lithium compound.

Overall, 2D membranes have advanced from size-dependent ion transport towards the coordinated regulation of solvation, electrostatics, chemical recognition and channel integrity. Li^+/Mg^{2+} separation is comparatively mature, whereas Li^+/Na^+ and Li^+/K^+ discrimination remains strongly dependent on ion-specific recognition or selective removal of competing ions. Most studies demonstrate selective transport or enrichment in model solutions, artificial seawater or lithium-rich brines. The transition to practical seawater recovery will require stable operation at trace lithium concentrations, regeneration, closed mass balances and integration with downstream lithium-product formation.

3.2. Uranium Separation and Recovery

Uranium recovery from seawater is intrinsically challenging because of its ultralow concentration, complex aqueous speciation and overwhelming excess of competing ions. Under marine carbonate conditions (pH ≈ 8), uranium does not exist as the free uranyl ion (UO_2^{2+}) but predominantly as bulky uranyl–carbonate complexes: the multivalent triscarbonato anion $[UO_2(CO_3)_3]^{4-}$, together with calcium-uranyl species—the neutral $Ca_2UO_2(CO_3)_3(aq)$ and the negatively charged $CaUO_2(CO_3)_3^{2-}$, which form by association with the abundant Ca^{2+} ions of seawater. Size-sieving considerations therefore apply to these large molecular complexes rather than to the bare uranyl ion. An effective membrane must combine molecular-scale channel regulation with specific recognition of uranyl–carbonate species, while maintaining permeability and structural integrity in a high-ionic-strength environment.

Early GO membranes used protonation and oxidation to suppress swelling and tune channels for uranyl separation in acidic radioactive waste [64]. As illustrated in Figure 6A, increasing acidity protonates oxygen-containing groups and weakens intersheet electrostatic repulsion, whereas the oxidation degree provides an additional means of regulating the wet basal spacing (d = 11.4–15.5 Å). The resulting contraction of the lamellar galleries progressively restricts the permeation of UO_2^{2+} relative to K^+ and Sr^{2+}.

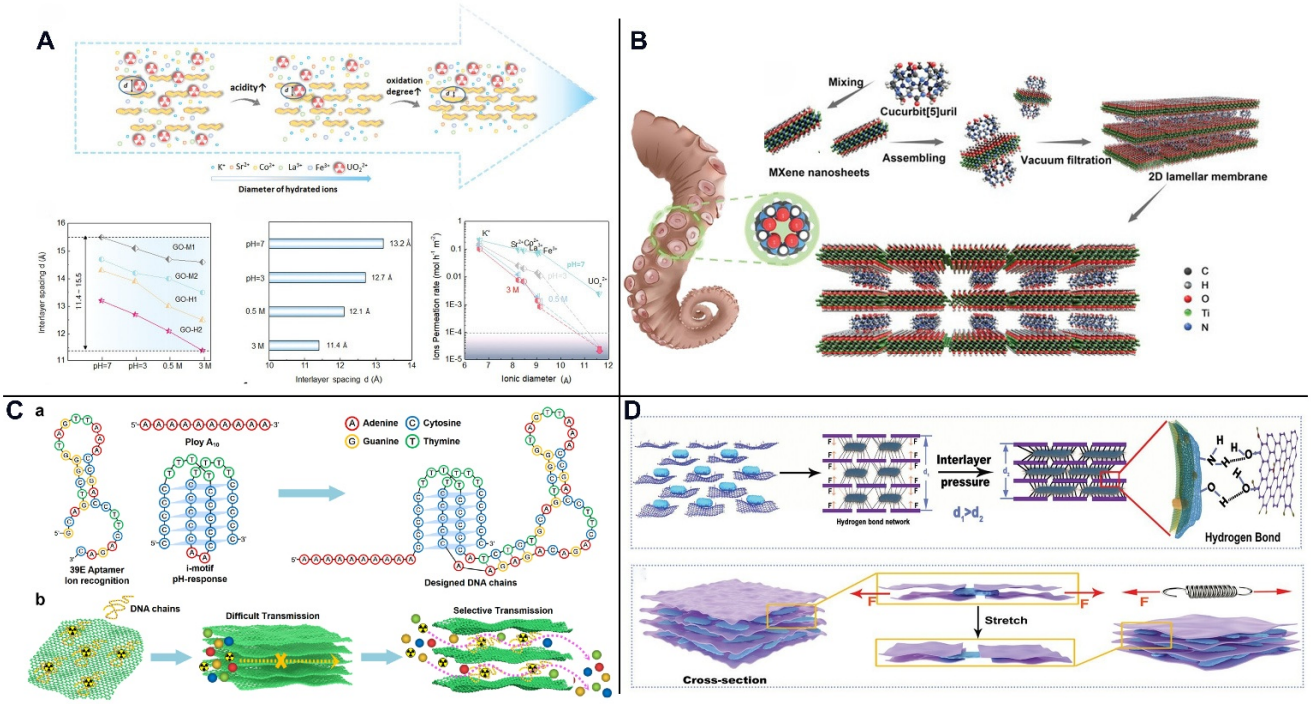


Figure 6. (**A**) Acidity– and oxidation–dependent regulation of graphene oxide interlayer spacing for uranyl sieving from acidic radioactive waste. Reprinted from [64]. (**B**) Cucurbituril–riveted [5] $Ti_3C_2T_x$ galleries for suppressing salt–induced swelling and enriching uranyl carbonate. Reprinted

from [65]. (**C**), a: pH–responsive i–motif gating and uranyl-specific aptamer recognition, b: DNA-intercalated graphene oxide channels integrating poly$(A)_{10}$ anchoring. (**D**) Charge–assembled GO/uranium–recognition–bacteria membranes combining hydrogen–bond–mediated structural reinforcement with specific uranyl coordination and confined transport.

Intercalation of metal–organic frameworks further introduced size-selective cavities and coordination sites into GO laminates. Cu-BTC/GO and Zn-BTC/GO membranes, for example, exhibited preferential discrimination between uranyl and competing multivalent ions, with the latter showing a Th^{4+}/UO_2^{2+} selectivity of approximately 25 [66]. These results establish the feasibility of coupling interlayer confinement with coordination chemistry for uranium separation, although the acidic or simplified feed solutions used in these studies differ substantially from seawater speciation.

More seawater-oriented designs have focused on stabilizing lamellar channels and introducing uranyl-recognition sites. Cucurbituril-riveted $T_3C_2T_x$ MXene membranes combined rigid molecular pillars with negatively charged transport pathways (Figure 6B) [65]. The optimized membrane retained more than 97.5% of uranyl species in simplified solutions while maintaining a water permeance of approximately 45 L m^{-2} h^{-1} bar^{-1}. Biomimetic functionalization provides a complementary route that relies less exclusively on steric exclusion. Incorporation of uranium-binding DNA aptamers into GO laminates created specific coordination and confinement sites that restricted uranyl transport while preserving water permeation (Figure 6C) [67]. The resulting membranes maintained high uranium rejection over repeated filtration cycles and showed antibacterial activity, which may help mitigate biofouling during marine operation. Similarly, genetically engineered microorganisms expressing uranyl-binding proteins have been assembled with GO nanosheets to form bio-inorganic lamellar membranes (Figure 6D) [68]. These architectures combine selective uranyl coordination with mechanically confined transport pathways and have demonstrated discrimination against vanadium and abundant alkali ions. Nevertheless, the long-term stability and degradation kinetics of aptamer-based biological recognition motifs must be critically considered for practical deployment. Marine biofouling and ambient microbial activity in real seawater may degrade aptamer sequences and deteriorate recognition performance over extended operational periods.

Collectively, current studies demonstrate that two-dimensional membranes can selectively retain or concentrate uranium-containing species by integrating channel stabilization, charge regulation and affinity recognition. However, high rejection should not be equated with uranium recovery. In most reported configurations, uranium accumulates in the retentate or at binding sites within the membrane, whereas desorption, product purification, membrane regeneration and uranium mass balance are rarely evaluated as an integrated process. Future work should move from short-term rejection experiments toward continuous cross-flow concentration using natural seawater, followed by low-chemical-demand elution and repeated adsorption–desorption or filtration–regeneration cycles. Particular attention should be given to uranium speciation, competition from carbonate and vanadium, organic fouling and the attainable concentration factor, since these parameters ultimately determine whether selective transport can be translated into recoverable uranium products.

3.3. Caesium Separation and Recovery

High rejection or apparent selectivity in laboratory tests should not be equated with practical recovery of the target ion from complex real feeds. Caesium separation is primarily relevant to the decontamination of seawater and saline radioactive effluents, although concentrated brines may also represent a potential secondary resource. Its separation is complicated by the similar monovalent character of Cs^+, K^+, Rb^+ and Na^+, as well as the high abundance of competing alkali ions. Because hydrated Cs^+ undergoes relatively

weak hydration, purely size-based nanochannels generally provide insufficient selectivity. Caesium-selective membranes require host–guest recognition, ion exchange or precisely regulated coordination environments in addition to dimensional confinement.

Ammonium molybdophosphate-modified GO membranes achieved 99.2% Cs rejection in simplified feed water and retained 87.4% rejection in real seawater, with stable performance over five cycles [69]. In these composites, GO provides a permeable lamellar framework, whereas ammonium molybdophosphate introduces Cs-selective ion-exchange sites. Caesium removal was attributed to NH^{4+}/Cs^{+} exchange and inner-sphere coordination within the immobilized inorganic phase. This design effectively suppresses the loss of fine ion-exchange particles and couples adsorption with pressure-driven filtration. Nevertheless, the process remains capacity-limited, and its practical applicability depends on the regeneration of the ion-exchange phase and the management of concentrated radioactive eluates.

Molecular recognition has also been introduced through crown-ether intercalation. Dibenzo crown ether-modified GO membranes displayed approximately 94.4% Cs rejection and a water permeance of 15.8 L m^{-2} h^{-1} bar^{-1}, while showing lower rejection toward Rb^{+}, K^{+} and Na^{+}. In a Cs/Na mixed solution, a separation factor of approximately 5 was reported [70]. The simultaneous increase in Cs rejection and water permeability indicates that appropriately selected molecular spacers can regulate both channel dimensions and ion–channel interactions.

Structurally stabilized carbon-based membranes provide another strategy for Cs-containing radioactive waste. Non-swelling oxidized graphene-ribbon membranes maintained fixed nanochannels in acidic multicomponent solutions and produced Cs/U separation factors exceeding 10^3, whereas reduced-GO membranes have enabled rapid Cs transport relative to Co and other transition-metal ions [71]. More recently, coordination–occupation coupling in polyacrylate-confined vermiculite membranes allowed Cs^{+} transport while suppressing Sr^{2+}, La^{3+} and Zr^{4+}, yielding Cs/Sr separation factors approaching 10^3 [72]. These studies highlight the importance of matching membrane transport direction to the intended process: Cs rejection enriches the retentate, whereas preferential Cs permeation produces a permeate-enrichment configuration. At present, however, most evidence supports Cs decontamination or selective partitioning rather than resource recovery. Continuous concentration, radionuclide-safe regeneration and quantitative Cs mass balances remain necessary before such membranes can be considered recovery technologies.

When evaluating published membrane performance, it is essential to clarify process topology: many reported membranes operate in rejection mode, achieving retentate enrichment of target Cs^{+}, while fewer systems operate in selective-permeation mode to extract Cs^{+} into the permeate stream. These two configurations correspond to completely different process workflows for resource recovery.

3.4. Strontium Separation and Recovery

Strontium separation from seawater is governed by strong competition from chemically similar alkaline-earth ions, particularly Ca^{2+} and Mg^{2+}. For radioactive ^{90}Sr, the principal objective is usually decontamination rather than resource recovery, whereas stable strontium recovery would require separation from the much larger divalent-ion background. Because Sr^{2+} has no distinctive charge state and only modest differences in hydrated size and hydration energy, electrostatic exclusion alone is generally insufficient. Selective transport must instead exploit narrowly regulated channel dimensions, differential dehydration barriers or Sr-specific coordination.

Existing two-dimensional membrane studies have largely been conducted in radioactive-waste matrices. Polyethylenimine-modified GO membranes form positively charged, acid-responsive nanochannels that permit monovalent ions such as Li^{+}, K^{+} and Na^{+} to pass

while suppressing Sr^{2+} transport, even under strongly acidic conditions [73]. Non-swelling oxidized graphene-ribbon membranes similarly preserved their channel structure in acidic multicomponent feeds and achieved a Sr/U separation factor of approximately 2705 [71]. These results demonstrate the value of covalent stabilization and charge regulation for radionuclide partitioning but do not establish selectivity between Sr^{2+} and the dominant alkaline-earth ions in seawater.

An alternative process topology is to promote Sr^{2+} permeation while retaining competing transition-metal ions. Amino-hydrothermally reduced GO membranes exhibited Sr/Co, Sr/Ni and Sr/Zn separation factors of 3232, 4254 and 3314, respectively, together with a water permeance of approximately 50.3 L m^{-2} h^{-1} bar^{-1}. The preferential transport of Sr^{2+} was attributed to its comparatively lower energetic penalty for entering narrow hydrophobic nanochannels, whereas Co^{2+}, Ni^{2+} and Zn^{2+} experienced stronger dehydration and distortion barriers [74]. This mechanism illustrates that selective separation does not necessarily require complete target-ion rejection; preferential permeation can also be useful if the receiving stream is designed for subsequent concentration.

Hybridization with porous coordination frameworks has further expanded the available recognition mechanisms. Polyethylenimine-assisted UiO-66-NH_2/GO membranes combine controlled interfacial channels, electrostatic repulsion and size exclusion, resulting in high Sr rejection across variations in concentration, pH and competing-ion composition, while improving Cs/Sr separation [75]. Surface-functionalized GO membranes and GO–crown ether composites have also shown substantial Sr adsorption capacities, but these systems operate predominantly as membrane-supported adsorbents rather than continuous molecular sieves [76]. These transition-metal selectivities, however, do not directly address the ions that dominate natural brines: the abundant alkaline-earth ions Ca^{2+} and Mg^{2+}, which resemble Sr^{2+} in charge and hydrated size and far exceed it in concentration, constitute the principal interference for strontium recovery. Reported Sr/transition-metal ratios should therefore not be taken as evidence of selectivity against the actual brine matrix.

Overall, the current evidence supports the feasibility of Sr decontamination from acidic nuclear waste but remains insufficient for selective recovery from seawater. In particular, Sr/Ca and Sr/Mg discrimination under realistic salinity has rarely been demonstrated, and studies often report rejection or binary separation factors without determining the concentration and purity of the collected Sr stream. Advancing toward recovery will require affinity sites capable of distinguishing alkaline-earth ions, stable cross-flow operation in natural seawater and regenerable capture or downstream concentration of the Sr-enriched fraction. Until these requirements are met, most reported systems should be described as selective Sr transport, retention or decontamination rather than strontium recovery.

3.5. Rubidium and Other Underexplored Ions

Rubidium represents a particularly demanding target because its hydrated dimensions and monovalent charge closely resemble those of K^+, while its concentration in seawater is substantially lower. Conventional charged nanochannels cannot readily discriminate between these ions, and the large excess of K^+ magnifies even minor losses in selectivity. Accordingly, Rb recovery requires sub-ångström control over channel geometry or recognition sites capable of resolving subtle differences in dehydration and ion–surface interactions.

Early ion-transport studies illustrate this limitation. Acid-functionalized covalent organic framework membranes enabled rapid monovalent-ion transport, but Rb^+ and K^+ exhibited similar diffusion behaviour and were not effectively separated from each other [77]. Crown ether-intercalated GO membranes produced different rejection values for Cs^+, Rb^+, K^+ and Na^+, indicating that molecular recognition can partially differentiate closely related

alkali ions; nevertheless, these membranes were optimized for Cs rejection rather than selective Rb recovery [70].

A major advance was recently achieved using polydopamine-pillared GO membranes with precisely controlled interlayer spacing. Batch regulation of the nanochannels within the sub-ångström range enabled discrimination between hydrated Rb^+ and K^+, whose effective dimensions differ by less than 0.1 Å, and produced a reported Rb/K separation factor of 5320. The membrane also maintained stable water transport during extended operation, demonstrating that highly confined lamellar channels can resolve ion-size differences previously considered inaccessible to conventional membrane sieving [78]. This result establishes an important mechanistic benchmark, but it does not yet constitute seawater Rb recovery: performance at the native Rb/K concentration ratio, the identity of the Rb-enriched stream, attainable concentration factors and product recovery were not evaluated as a complete process. Sub-ångström channel engineering does not discriminate between closely related alkali ions solely according to their hydrated radii. When the channel width approaches the dimensions of the first hydration shell, permeation requires partial dehydration and reorganization of confined water, generating an entry barrier governed by ion–water binding and the stabilization of the partially dehydrated ion by the channel walls. Because permeability depends exponentially on this activation barrier, even small differences in dehydration free energy can produce pronounced selectivity between Rb^+ and Cs^+. Sub-ångström tuning therefore creates a critical transport regime in which one ion preferentially permeates because of its lower partial-dehydration penalty, whereas wider channels transmit both ions and excessively narrow channels exclude both.

Considerably less documentation exists for other high-value ions, including rare-earth elements, vanadium and selected transition metals. Existing two-dimensional membranes generally use these ions as competitors in uranium separation or as model solutes in radionuclide-remediation studies. Future research should prioritize realistic multicomponent feeds, target-to-background selectivity rather than binary selectivity alone, and integrated concentration–regeneration processes. For Rb and other underexplored ions, the central research gap has shifted from demonstrating molecular-scale discrimination to proving that such discrimination can generate a sufficiently concentrated and recoverable product under authentic seawater conditions.

4. Performance and Design of 2D Membranes

Two-dimensional materials provide a broad and increasingly diverse platform for constructing ion-selective membranes. The main 2D material families include graphene oxide and its derivatives, MXenes, transition-metal dichalcogenides, two-dimensional COFs and MOFs, layered clays, layered double hydroxides and heterolamellar or composite membranes, as shown in Figure 7. These materials form interlayer galleries, intrinsic framework pores or in-plane nanopores and offer different combinations of channel tunability, surface chemistry, charge regulation, structural stability and processability.

4.1. Graphene Oxide and Derivative Lamellar Membranes

Graphene oxide (GO) is among the most extensively investigated 2D platforms for ion separation. Its nanosheets contain both aromatic carbon domains and oxygenated functionalities, and their stacking generates elongated 2D interlayer channels. The graphitic regions can reduce friction for water and selected permeating species, whereas carboxyl, hydroxyl and epoxide groups provide hydrophilicity, negative charge and reactive sites for further functionalization [79]. This coexistence of physical confinement and chemically heterogeneous interfaces enables GO membranes to combine interlayer sieving, cation–π

interactions, electrostatic partitioning and functional-group coordination rather than relying on size exclusion alone [80].

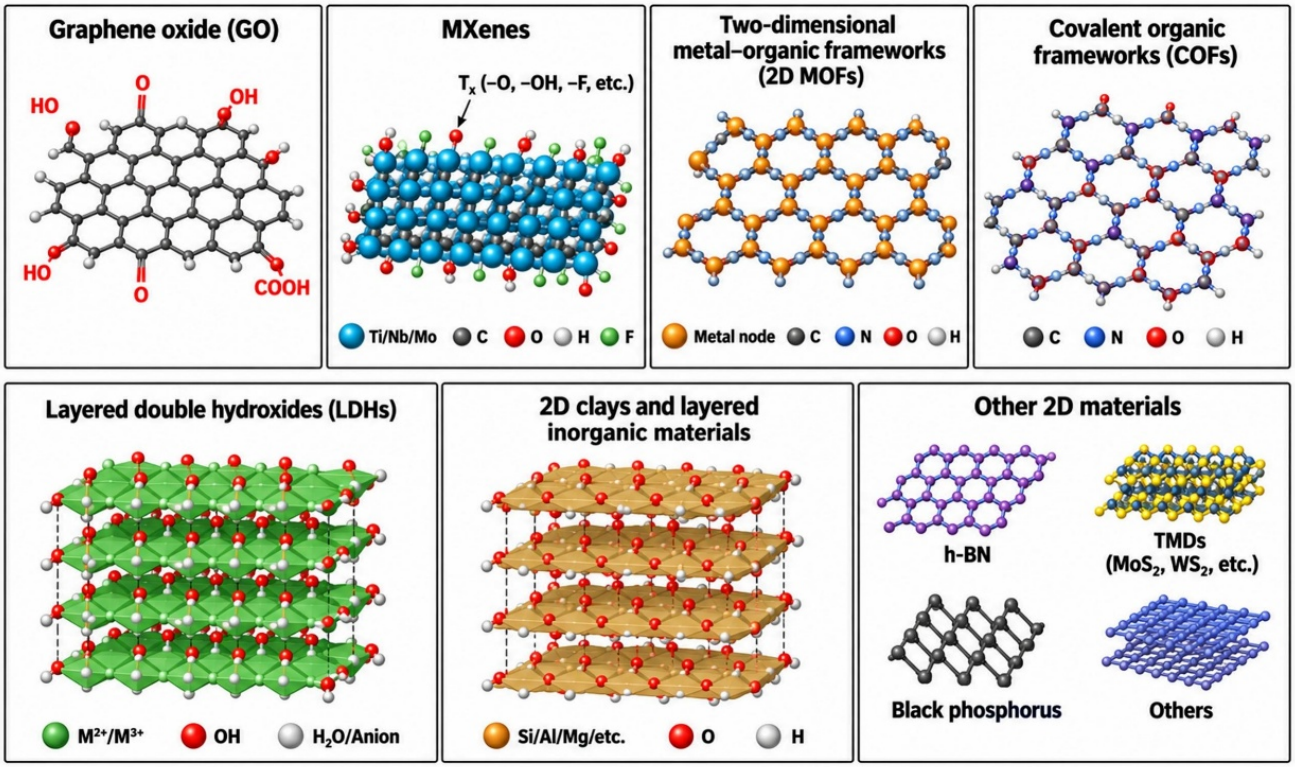


Figure 7. Typical two-dimensional layered membranes for ion separation.

The principal strengths of GO are its processability and structural tunability. Continuous selective layers can be fabricated by vacuum filtration, coating, spraying or interfacial assembly, while crosslinking, ionic intercalation, polymer insertion and partial reduction offer multiple routes to adjust the interlayer spacing and channel chemistry. Chen et al. achieved ångström-level control of the GO interlayer spacing through cation-dependent interactions with oxidized and graphitic domains, thereby excluding ions with larger hydrated dimensions [16]. Abraham et al. suppressed excessive swelling through physical confinement, shifting the ion-sieving cut-off toward the hydrated-ion scale, but also observed an exponential reduction in permeation as the channels narrowed [18]. These studies established GO as a tunable interlayer sieve while exposing an intrinsic tension between structural precision and transport rate.

The main weakness of GO arises from the same hydrophilic and dynamic structure that makes it tunable. Water uptake expands the gallery spacing, whereas salinity, pH, cation identity and pressure alter the interactions between neighbouring sheets. Consequently, a dry-state spacing measured by X-ray diffraction cannot be equated with the effective aperture during operation. Under nanofiltration conditions, moreover, transmembrane hydraulic pressure gradients exceeding approximately 10–20 bar can progressively compact reduced or functionalized GO laminates: the sustained load expels interlayer water, reduces the gallery height and densifies the stack during long-term operation, which lowers permeance and can shift the effective sieving aperture away from the designed value. Pressure-induced compaction therefore acts as an additional time-dependent channel-stabilization constraint that must be considered alongside swelling when selecting the operating pressure. Edge gaps, wrinkles, cracks and interfaces with the support may additionally create non-selective routes that bypass the intended interlayer channels. Conversely, stabilization by dense

crosslinking or extensive reduction can obstruct low-resistance pathways and sharply decrease permeance [17].

Recent work has shifted from indiscriminate compaction toward spatially selective pillaring. In 2026, Lu et al. reported polydopamine-pillared GO membranes in which the disparate time scales of rapid dopamine assembly and slower chemical reaction were exploited to support oxidized regions while preserving fast transport through carbon-rich domains [78]. The hydrated interlayer spacing could be tuned within the sub-nanometre regime, and the membranes remained stable under cross-flow operation. Increasing the aqueous spacing from 6.5 to 9.0 Å raised the water permeance from 49.1 to 104.3 L m^{-2} h^{-1} bar^{-1}, while decreasing NaCl rejection from 99.8% to 65.2%, directly quantifying the trade-off between channel accessibility and ion exclusion [78]. Li-related separation was demonstrated using pretreated seawater, and a dual-membrane configuration enriched Rb^+ relative to the closely similar K^+ ion. These results extend the resolution attainable with GO membranes. However, the use of a pretreated feed and a multistage arrangement means that overall recovery, energy demand and tolerance to untreated seawater remain to be established.

GO is thus particularly attractive when large-area fabrication, continuously adjustable interlayer spacing, and diverse functionalization routes are required. Its central limitation is not a lack of tunability, but the difficulty of converting tunability into a reproducible operating-state structure under high salinity, sustained pressure and long-term exposure. The practical competitiveness of GO will depend on whether wet-state aperture characterization, low-resistance stabilization, and defect control can be achieved simultaneously.

Reduced or functionalized graphene oxide laminates are susceptible to irreversible long-term compaction under hydraulic pressure drops exceeding 10–20 bar in nanofiltration operating modes. Such compaction compresses interlayer galleries and progressively lowers water permeance during continuous high-pressure filtration, which represents a critical stability concern for real-scale seawater and brine processing.

4.2. MXene Lamellar Membranes

MXenes, most commonly represented by $Ti_3C_2T_x$, carry surface terminations such as –O, –OH and –F and generally exhibit high hydrophilicity and adjustable surface charge. Relative to GO, their inorganic backbone, termination chemistry, and electronic conductivity enable both passive interlayer sieving and active regulation through applied potentials, reversible protonation or electrochemical control [81–83]. Early work by Ren et al. demonstrated charge- and size-selective transport through $Ti_3C_2T_x$ membranes [84], and subsequent studies used self-crosslinking, polymer intercalation and ionic or molecular decoration to regulate spacing, charge, and confined water content [20,85].

A distinctive advantage of MXene membranes is their responsive interfacial chemistry. Protonation states can be varied with pH, thereby changing ion partitioning, while the conductive framework permits the channel charge environment to be modulated electrically. Reversible pH gating and voltage gating have shown that mono-/divalent selectivity and even the transport sequence among monovalent cations can be altered within the same membrane [86,87]. Such adaptive behaviour is attractive for brines of variable composition because selectivity can be adjusted during operation rather than being fixed entirely during synthesis. Nevertheless, external control also increases process complexity. Local electric fields, concentration polarization and electrode reactions can prevent selectivities measured in small laboratory cells from being transferred directly to continuous modules.

Strong intersheet interactions can provide MXenes with greater resistance to swelling, but they do not eliminate structural evolution in water. Self-crosslinked $Ti_3C_2T_x$ membranes improve antiswelling behaviour [81], whereas $Ti_3C_2T_x$/alginate and $Ti_3C_2T_x$/PSS archi-

tectures stabilize channels through sheet immobilization and polymer confinement and have been used for general ion sieving or preferential Li^+ transport [56,83]. Noncovalent decoration and biomimetic subnanochannels further show that molecular occupancy, local charge and the hydration state within the gallery collectively determine selectivity [85]. MXene membranes should be regarded as dynamic nanofluidic systems involving surface terminations, intercalants, confined water and external fields, rather than as simple charged slits.

The principal risks of MXene are chemical instability and structural reorganization. $Ti_3C_2T_x$ can progressively oxidize in oxygenated water, and the termination composition varies with synthesis and storage history. Oxidation initiates preferentially at flake edges and defect sites and ultimately converts $Ti_3C_2T_x$ into TiO_2 together with amorphous carbon, degrading electrical conductivity and channel integrity. To counter this degradation in oxygenated aqueous environments, specific protection strategies have been proposed, including the addition of antioxidants such as sodium L-ascorbate or citric acid to the dispersion or feed solution and covalent edge passivation that caps the reactive edge sites; both approaches retard oxidative damage during fabrication, storage and long-term operation. Restacking, variations in flake size and oxidation products all modify effective transport pathways. Recent studies consequently treat lateral size, orientation and channel water content as independent design variables rather than focusing exclusively on mean interlayer spacing [50,88]. Nominally identical compositions can thus yield membranes with substantially different transport behaviour. For recovery applications, flake batch, termination composition, oxidation state, hydrated spacing and long-term electrochemical stability must be reported if material–performance relationships are to be reproducible. A key practical bottleneck for MXene membranes is aqueous oxidative degradation towards titanium-dioxide phases in dissolved-oxygen-containing feeds. Specific preservation strategies, such as antioxidant addition or covalent edge-capping modifications, can mitigate this oxidative degradation, thereby extending service lifetime under continuous real-brine operation.

MXenes are particularly suited to separations that benefit from coupled electric fields, responsive charge or interlayer chemical modification. For ion pairs with different valence, such as Li^+/Mg^{2+}, charge exclusion can work synergistically with confinement. For same-valence pairs such as Li^+/Na^+ or Li^+/K^+, however, electrostatics alone is rarely sufficient, and more precise control of dehydration or ion-specific recognition is required. MXene is better understood as a programmable channel scaffold than as a material with an intrinsic preference for a particular valuable ion.

4.3. Graphene, MoS_2 and Other In-Plane Nanoporous Membranes

Single- or few-layer graphene and MoS_2 membranes provide nearly perpendicular, ultrashort transport paths through in-plane nanopores. Their primary advantage is exceptionally low geometric resistance. Both simulations and experiments indicate that an atomically thin pore can combine steric exclusion, partial dehydration and entrance chemistry when its aperture approaches the hydrated-ion scale and its edge carries an appropriate charge [89,90]. Compared with the extended and tortuous pathways of lamellar membranes, in-plane pores can increase the transport rate per pore and enable relatively direct correlations between pore-entry free-energy barriers and selectivity.

In practice, single-layer nanoporous membranes cannot operate as freestanding structures; mechanical-support interlayers are required for large-area fabrication. Substrate pore coverage is another important variable: nonuniform substrate coverage can create dead zones and directly modulate the effective target-ion flux of the composite membrane system, which must be accounted for when extrapolating laboratory fluxes to real feed processing.

The shortest pathway does not necessarily provide the greatest ion–ion discrimination. Hoenig et al. generated sub-nanometre-to-nanometre pores in MoS_2 in situ and found that smaller pores enhanced the selectivity of KCl over NaCl, LiCl and divalent salts [89]. Experiments and molecular dynamics suggested that ion dehydration, surface-charge screening, and ion–ion coupling act together in narrow multilayer pores. In a monolayer aperture, the path may be too short to fully disrupt an ion's hydration shell because water molecules outside the membrane can partly sustain it. Membrane thickness determines not only resistance but also the integrated interaction length over which competing ions can be distinguished.

For MoS_2, covalent functionalization of lamellar structures provides one means of adjusting both spacing and surface chemistry [90], while in-plane membranes can be tuned through pore-size, edge-termination and grain-boundary engineering. Grain-boundary engineering in monolayer MoS_2 reported in 2025 further suggested that boundaries can be transformed from uncontrolled defects into dense, deliberately designed transport pathways [91]. Engineering limitations nevertheless remain severe. Producing atomically thin membranes with a narrow pore-size distribution, high pore density and mechanical integrity over areas ranging from centimetres to square metres is difficult. A small number of oversized pores can dominate leakage, while pore contamination or chemical reconstruction can amplify device-to-device variability. Mechanical support adds a further constraint. Atomically thin layers cannot remain freestanding over macroscopic areas, so a mechanically supporting interlayer, typically a porous substrate, is indispensable. This support, however, introduces its own series hydraulic resistance and geometric bottleneck. The pore coverage, or open porosity, of the substrate determines the fraction of the nominal membrane area that actively contributes to transport. Where the substrate is impermeable, the nanosheet cannot allow permeation; a low-porosity support therefore confines the effective target-ion flux to the regions above its pores, making the area-normalized flux a property of the substrate architecture as much as of the pore chemistry of the nanosheet. Membrane benchmarking should consequently report both support porosity and selective-layer pore statistics.

Other 2D materials, including hexagonal boron nitride, offer potentially useful combinations of chemical stability, tunable surface charge and low-friction interfaces. Direct membrane-level evidence for recovering valuable ions from seawater or brine is, however, less mature than that for GO, MXenes, and COFs. These materials currently serve more convincingly as platforms for mechanistic inquiry and future development than as application-ready comparators.

4.4. Two-Dimensional COF and MOF Membranes

Two-dimensional covalent organic frameworks (COFs) and metal–organic frameworks (MOFs) combine ordered pores with programmable chemistry and offer a distinct route to separating ions with closely similar physical properties. Unlike GO and MXene laminates, in which transport occurs primarily through intersheet galleries, COF and MOF architectures can define aperture size, ligand identity, fixed charge, and recognition sites during framework synthesis. They can reduce chemical heterogeneity and distribute ion-partitioning and dehydration barriers along ordered pathways [36,42,57,77,92].

An important advance in COF membranes has been the transition from single-aperture sieving to serial control by chemically distinct pore regions. Phosphonic-acid-containing COFs can create hydrophilic acidic domains in which bound water forms a locally confined transport stage, while adjacent nonacidic domains retain lower resistance, thereby coupling enthalpic and entropic contributions to monovalent-ion selectivity [77]. Amino-acid-functionalized COFs have exhibited switchable Na^+/K^+ selectivity, demonstrating that the chemical state of a recognition group can reorder the transport preference among same-valence ions [92]. Modulation of pore solvation further changes the balance be-

tween dehydration and the stabilization inside the framework [57], while a randomly oriented sulfonated COF membrane combined orientation-induced narrow channels with ion–functional-group interactions to distinguish Li^+ from competitors under an electric field [42]. The significance of COFs extends beyond pore-size uniformity to encompass their ability to spatially arrange hydration microenvironments, fixed charges and recognition sites along a continuous transport pathway.

Two-dimensional MOF membranes analogously modulate electrostatic and coordination microenvironments via their metal nodes and organic linkers. Concurrently regulating ion affinity and dehydration barriers within sub-nanometre MOF channels has enabled the discrimination of ion entry and subsequent migration [36]. Sulfonated 2D MOFs and MOF-intercalated GO membranes further show that a MOF can either form the selective pathway itself or function as a pillar and recognition element within a lamellar host [66,93]. For valuable ions, the key opportunity is the recognition of complex species or specific coordination geometries rather than generic valence exclusion alone.

The limitations of COF and MOF membranes arise from the gap between an ideal crystal model and an operating membrane. Grain boundaries, amorphous regions, orientation distributions, stacking offsets and support interfaces create pathways that differ from the crystallographic pore. To suppress the non-selective intercrystalline grain-boundary voids that arise in polycrystalline films, symbiotic synthesis strategies have been developed, notably gel-assisted and vapour-assisted growth. Gel-assisted routes grow the framework within a gel matrix that confines nucleation and bridges adjacent crystalline domains, promoting continuous, defect-healed films; vapour-assisted conversion exposes a pre-deposited precursor layer to monomer and catalyst vapours under controlled conditions, enabling high crystallinity and compact, pinhole-reduced membranes. Both approaches aim to narrow the gap between the ideal crystallographic pore and the operating membrane by minimizing grain-boundary leakage. High charge or functional-group densities may also retain ions so strongly that static affinity fails to produce steady-state permeation. Some frameworks undergo hydrolysis, ligand exchange or structural rearrangement in strongly acidic, alkaline, or saline media. Crystallographic pore dimensions must be evaluated together with membrane-level defect statistics, wet-state structures and extended permeation tests.

COF and MOF membranes are best positioned for tasks requiring high chemical resolution, including same-valence ion recognition and the discrimination of complexed species. Their future advantage depends on translating molecular programmability into reproducible pathways in large-area membranes while retaining the chemical integrity and reversibility of recognition sites during high-salinity operation and regeneration.

4.5. Layered Clays, LDHs and Related Inorganic Laminates

Layered clays such as vermiculite and montmorillonite combine low raw-material cost with relatively robust inorganic frameworks. Permanent layer charge, exchangeable interlayer ions and hydration-dependent swelling allow these materials to exhibit ion-affinity differences and to be tuned by pillaring and ion exchange. Two-dimensional clay membranes have shown intrinsic cation recognition [94], while self-confined vermiculite channels have demonstrated rapid Li-selective transport [95].

Hydration-induced swelling remains a central obstacle for layered clays, but the inexpensive inorganic backbone creates stabilization options distinct from those available to GO. Liu et al. introduced alumina pillars into vermiculite galleries, strengthening intersheet cohesion and water stability. By altering the sequence of Na^+ incorporation, they further adjusted surface charge and steric confinement so that the same platform could favour Li^+ over multivalent ions or over other monovalent ions [96]. The broader significance is that

the combination of pillar, exchange ion and layer charge can convert a nominally passive inorganic laminate into a programmable ion channel.

One critical failure mode for clay- and vermiculite-based membranes is irreversible gallery collapse triggered by deep dehydration events. Once the interlayer galleries fully collapse, the original nanochannel architecture cannot be recovered upon rehydration, leading to permanent loss of long-term water permeability. Operational protocols must therefore avoid complete drying of the membrane module.

A deeply dehydrated vermiculite membrane reported in 2026 used the removal of free and bound interlayer water to suppress reswelling and preserve narrow, ion-intercalated galleries during long-term operation [97]. Nevertheless, deep dehydration carries a structural risk: if the galleries collapse below a critical spacing during water removal, the interlayer channels may undergo irreversible collapse because the sheet–sheet interactions of the dehydrated clay prevent their re-expansion upon subsequent rehydration. Such an irreversible transition sharply reduces the accessible channel volume and therefore the water permeance, meaning that the long-term water-permeation performance of deeply dehydrated clay and vermiculite membranes must be monitored over repeated rehydration–dehydration and permeation cycles. A stable, reproducible channel aperture, rather than the lowest achievable d-spacing, should accordingly be the design target. The membrane was integrated with electrodialysis and precipitation to produce Li_2CO_3. Compared with studies limited to selectivity in model solutions, this chain of evidence, from structural stabilization and salt lake brine separation to product formation, is more consistent with the requirements of resource recovery. Its generality nevertheless requires validation across brine compositions, enlarged membrane areas and repeated operating cycles.

Layered double hydroxides (LDHs) contain positively charged sheets and exchangeable interlayer anions and are, in principle, attractive for anion-selective transport or for regulating lateral and transverse pathways in composites. Direct evidence for membrane-based recovery of cationic resources such as Li, Rb, Cs, or Sr remains limited. Their current value lies mainly in high charge density, inorganic stability, and use as a component of heterogeneous channels. Membership in the 2D material family should not itself be taken as evidence of target-ion selectivity; the selective transport function of the LDH must be demonstrated in the membrane architecture.

4.6. Heterolamellar and Composite 2D Membranes

A single material rarely provides precise selectivity, high transport rate, wet-state stability, and scalable fabrication simultaneously. Heterolamellar membranes combine two or more types of 2D sheet, polymer, or porous crystal so that structural support, ion recognition, defect sealing, and rapid transport can be assigned to different components. GO/MXene, GO/MOF, vermiculite/MOF, and 2D-material/polymer composites all illustrate this strategy [98].

The genuine value of heterogeneity is functional spatial separation rather than an increased number of constituents. One component can immobilize the spacing, another can regulate target-ion partitioning, a conductive phase can provide electric-field responsiveness, and a continuous 2D scaffold can preserve mechanical integrity. Recent work on 2D heterogeneous channels used charge locking to regulate both gallery structure and the local electrostatic environment, establishing channel heterogeneity as an independent design variable for Li separation from brine [98]. Such architectures move beyond optimization of a single mean spacing and more closely reflect the spatially nonuniform pathways present in real membranes.

Heterogeneity can introduce interfacial voids, local delamination, nonuniform composition, and batch variability. If selectivity originates from a small population of high-affinity

sites, site saturation or fouling may also occur during prolonged operation. A composite membrane must demonstrate mechanistic synergy rather than simple performance addition. Single-component controls, interface characterization, pathway validation, and long-term tests are needed to identify the role of each component and to exclude leakage through newly created interfaces.

Real feeds impose additional constraints on the long-term operation of heterolamellar and composite membranes. Fouling, inorganic scaling and hydration-induced swelling may increase transport resistance or alter the effective nanochannel dimensions, whereas the functional groups responsible for charge-based selectivity may also act as adsorption or nucleation sites. Surface modification, interlayer cross-linking and stronger selective-layer/support interactions are therefore required to balance ion selectivity, structural stability and fouling resistance [99,100].

At the module level, integrating ultrathin 2D selective layers with porous hollow-fibre supports is a promising scale-up route because hollow fibres provide high packing density, short transport distances and compatibility with continuous cross-flow operation. Polyamine-functionalized GO hollow-fibre membranes have recently been assembled into 88 cm^2 modules, demonstrating improved underwater stability and compatibility with established hollow-fibre manufacturing processes [101]. $Ti_3C_2T_x$ MXenes have been assembled on polymeric hollow-fibre substrates for divalent-ion nanofiltration [102]. Nevertheless, these demonstrations remain largely at the laboratory scale, and validation using multi-component brines, controlled hydrodynamics and long-duration module operation is still required [103].

Table 2 summarizes the capabilities and limitations of the major 2D membrane families. GO and MXenes are comparatively mature in membrane formation and interlayer regulation; COFs and MOFs provide exceptional chemical programmability; atomically thin nanoporous membranes minimize geometric resistance; and clays offer potential advantages in cost and inorganic robustness. Materials must consequently be selected in relation to a defined separation task.

Table 2. Comparison of major 2D membrane platforms for selective ion transport.

Material Platform	Principal Pathway	Distinctive Capability	Most Relevant Tasks	Main Limitations	Typical Water Permeance Range
GO and derivatives	Intersheet slits and edge pathways	Scalable processing, adjustable spacing, rich functionalization	Size/dehydration control, functional recognition, mono-/multivalent separation	Swelling, defect leakage, salt- and pH-dependent structure	10–120
MXenes	Hydrophilic, charged interlayer channels	Tunable terminations, conductivity, pH and electric-field responsiveness	Charge-coupled separation, gated transport, composite stabilization	Oxidation, restacking, termination and batch variability	8–95
Graphene/TMD in-plane pores	Vertical atomically thin nanopores	Short path length and designable pore-entry chemistry	High-flux model separations and dehydration studies	Difficult large-area pore control; extreme sensitivity to oversized defects	20–180

Table 2. *Cont.*

Material Platform	Principal Pathway	Distinctive Capability	Most Relevant Tasks	Main Limitations	Typical Water Permeance Range
2D COFs/MOFs	Framework and interlayer pores	Programmable apertures and recognition sites	Same-valence ions, complexed species, ion-specific recognition	Grain boundaries, orientation, aqueous stability, continuous film formation	5–75
Clays/vermiculite/LDHs	Charged interlayer channels	Abundance, inorganic framework, ion exchange and pillaring	Low-cost mono-/multivalent separation and stable galleries	Hydration swelling, limited intrinsic specificity, uneven target-ion evidence	3–60
Heterogeneous/composite membranes	Mixed interlayer and interfacial pathways	Spatial allocation of stabilization, recognition and transport functions	Multi-mechanism separation, complex feeds, process coupling	Interfacial bypass, compositional nonuniformity, attribution and reproducibility	5–110

The comparison of major 2D membrane platforms indicates that no material offers a universal advantage across selectivity, permeability, stability, and manufacturability. Their suitability instead depends on whether the operating-state channel can amplify the relevant physicochemical contrast between the target and competing ions. Charge exclusion and dehydration provide a useful design window for mono-/divalent separations, whereas closely related monovalent ions require tighter control of channel dimensions, local solvation, or reversible coordination. For species with complex aqueous speciation, membrane design must further account for the charge and coordination state present in the actual feed. Material selection should proceed from the target ion pair and solution composition rather than from the nominal structure or intrinsic properties of an available 2D material [14,25,104,105].

Beyond the choice of material platform, the ion-separation performance of a 2D membrane is ultimately governed by its porous-structure features, which define the dominant transport pathway and the resulting selectivity. Table 3 correlates typical porous-structure features with their associated separation behaviours, covering in-plane intrinsic nanopores, restacked slit-shaped galleries, intercrystalline grain boundaries, and sheet-edge defects or pinholes. Because multiple structural features usually coexist in real membranes, this structure–performance comparison provides a practical reference for rational membrane design, fabrication quality control, and the interpretation of experimentally observed selectivity. Note that multiple structural features usually coexist in real-world 2D membranes; the overall separation output originates from the superposition of multiple transport pathways instead of a single structural feature.

Table 3. Correlation between membrane porous-structure features and ion-separation performance.

Porous-Structure Feature	Typical Structural Description	Associated Separation Behaviour	Explanatory Notes	References
In-plane intrinsic nanopores	Atomically thin sheet with discrete in-plane nanopores etched or intrinsically formed in nanosheets	High water flux; separation performance extremely sensitive to pore-size distribution	The transport path is atomically short; a small fraction of oversized defects will dominate leakage and degrade apparent ion-sieving selectivity	[48]

Table 3. *Cont.*

Porous-Structure Feature	Typical Structural Description	Associated Separation Behaviour	Explanatory Notes	References
Restacked slit-shaped galleries	Interconnected slit-like interlayer voids formed by physical stacking of two-dimensional nanosheets	Balanced trade-off between water flux and ion selectivity; highly prone to hydration-driven swelling in an aqueous environment	Wet-state aperture, rather than dry-state d-spacing measured by X-ray diffraction, determines practical sieving capability during operation	[16,18,20]
Inter-crystalline grain boundaries	Nanoscale void gaps existing between adjacent crystalline domains of polycrystalline COF/MOF membranes	Generate non-selective bypass flux and lower the apparent separation factor	Grain-boundary leakage can be suppressed via gel-assisted or vapour-assisted intergrowth synthesis techniques	[42]
Sheet-edge defects/pinholes	Local nanoscale pinholes, cracks and gaps distributed at sheet edges or within the nanosheet basal plane	Sharp deterioration of size-exclusion performance; real selectivity masked by defect-mediated unselective flow	Defect sealing and quality control are prerequisites for obtaining reliable intrinsic nanochannel-governed ion selectivity	[12,16]
Pillared or intercalated nanochannels	Interlayer galleries dimensioned or stabilized by molecular pillars, ionic intercalants or covalent crosslinkers inserted between adjacent nanosheets	Suppressed hydration swelling with a stable wet-state aperture; size/dehydration sieving combined with coordination- or charge-mediated selectivity	Pillars preferentially support oxidized or charged domains while preserving fast transport through unmodified regions; intercalation can simultaneously alter surface charge and affinity, so geometric and chemical contributions often act together	[12,31]
Heterolamellar interfacial channels	Interfacial pathways formed at junctions between different 2D sheets, porous crystals or polymers within heterolamellar or composite membranes	Multi-mechanism separation with spatially allocated stabilization, recognition and transport functions; charge-locked regulation of channel geometry	Heterogeneity can introduce interfacial voids and local delamination; mechanistic synergy rather than simple performance addition must be demonstrated to exclude leakage through newly created interfaces	[10]
Chemical recognition sites on channel walls	Crown ethers, oligoethers, EDTA, heteropolyacid ligands, DNA aptamers or amino-acid groups anchored inside the nanochannels	Ion-specific coordination resolves same-valence ions that size sieving alone cannot distinguish; recognition is coupled with nanoconfinement and local charge	Effective sites must balance selective partitioning, site-to-site migration and desorption; excessively strong binding converts transport sites into adsorption traps	[13,20]
Hydration-regulated wet-state galleries	Interlayer galleries whose operative dimensions evolve with water uptake, intercalated-ion valence, pH or applied pressure	Wet-state aperture governs practical sieving; swelling broadens the aperture distribution and lowers size-sieving precision, whereas dehydration or crosslinking can stabilize the channels	Dry-state XRD d-spacing does not represent the operative pore width during operation; operando characterization under feed conditions is required to establish structure–performance links	[12]

The translation of these molecular distinctions into recovery performance requires simultaneous control of hydrated channel structure, recognition-site accessibility, and non-selective defects. Stabilization should preserve the critical separation length scale without suppressing target-ion transport, while membrane fabrication must minimize swelling, interfacial voids, and batch-to-batch variability. Performance should also be assessed beyond membrane-level selectivity. Target-ion flux, enrichment, purity, recovery, stability, and energy consumption are collectively required to determine whether selective transport produces a useful product stream [106].

Table 4 summarizes representative quantitative performance data for 2D ion-selective membranes. Note that most performance data were acquired under laboratory conditions using simulated feed solutions. Selectivity and rejection values may deviate under authentic seawater or natural brine conditions due to complex competing-ion effects, charge-screening and membrane fouling. "Wet gallery" denotes interlayer spacing measured under hydrated operating conditions rather than dry-state X-ray diffraction results.

Table 4. Summary of representative quantitative performance data for 2D ion-selective membranes.

Membrane Material	Target Ion	Feed Solution Condition	Reported Selectivity	Recovery/Rejection Performance	References
MXene-PSS composite	Li^+	Artificial salt lake brine, multicomponent salt system	$Li^+/Mg^{2+} = 28$	Li^+ permeation rate: 0.08 mol m^{-2} h^{-1}	[56]
Crown ether-pillared ZHN	Li^+	Artificial seawater (25 μM Li^+ background, mixed alkali-metal ions)	$Li^+/Na^+ = 1422$	Target-ion enrichment in permeate (laboratory artificial feed, not a continuous real-seawater test)	[58]
Oxidized graphene-ribbon membrane	Cs^+	Acidic multi-ion radioactive simulant waste solution	$Cs^+/U > 1000$	Cs^+ rejection > 95%	[71]
Vermiculite coordination–occupation-coupled membrane	Cs^+	Simulated high-salinity brine containing Cs^+, Sr^{2+} and competing alkaline-earth ions	$Cs^+/Sr^{2+} \approx 1000$	Preferential Cs^+ permeation into the permeate stream	[72]
Polydopamine-pillared GO membrane	Rb^+	Multi-alkali-ion simulated brine containing Rb^+, K^+ and Na^+	$Rb^+/K^+ = 5320$	Rb^+ enrichment in retentate	[12]

5. Conclusions and Perspective

Future experimental reports should enforce standardised performance-reporting metrics, including energy consumption per kilogram of recovered target ion and comprehensive mass-balance calculations. These measurements are essential to rigorously distinguish genuine steady-state membrane-transport behaviour from temporary surface-adsorption or ion-exchange-driven enrichment artefacts.

This review has examined the selective separation of high-value ions from seawater and brines using two-dimensional membranes. It has connected ionic properties and aqueous speciation with transport mechanisms, target-specific separation behaviour, and the

characteristics of major 2D membrane platforms. The collective evidence indicates that ion selectivity is not an intrinsic attribute of a nominal pore size, functional group, or material class. Instead, it emerges from the coupled ion–solvent–membrane–electrolyte system under operating conditions. Hydrated size, dehydration energy, valence, polarizability, and coordination preference provide the physicochemical basis for ion discrimination. Their effects are mediated by channel geometry, confined water, interfacial charge, chemical affinity, and defect structure. Material selection must reflect the target–competitor pair, its solution chemistry, and the mechanism required to amplify their physicochemical differences.

Despite substantial progress in material design and mechanistic understanding, several challenges continue to limit the development of stable and predictable ion-selective 2D membranes: (1) Uncertain operating-state channel structure: Dry-state pore dimensions and interlayer spacings incompletely describe hydrated membranes. Water uptake, ion intercalation, surface protonation, pressure, and electric fields can reorganize channel dimensions and local interaction sites. (2) Ambiguous attribution of selectivity: Steric exclusion, dehydration, electrostatic partitioning, coordination, and defect-mediated leakage often operate concurrently. Their individual contributions remain difficult to separate, particularly at high ionic strength, where screening, ion pairing, and competitive adsorption alter the transport landscape. (3) Limited transferability to multicomponent feeds: Single-salt and dilute binary tests remain valuable for isolating mechanistic factors, yet they fail to capture the competitive speciation that characterizes seawater, brines, and concentrated industrial streams. The presence of competing ions, organic matter, and mineral precipitates can alter interfacial hydration layers, reduce the availability of binding sites, and modify the dominant transport pathways.

Resolving these challenges requires a coordinated methodological framework that connects hydrated-state structural dynamics, interfacial thermodynamics, ion-specific transport kinetics, and manufacturing variability. Operando and quasi-operando characterization should be performed under conditions directly comparable to transport measurements, thereby establishing causal links between channel reorganization and observed changes in ion selectivity. Computational models require constraints from experimentally resolved structures and should incorporate realistic hydration states, multicomponent electrolytes, chemical heterogeneity, and representative defect populations. Such models can quantify the relative contributions of dehydration, electrostatic partitioning, coordination and defect-mediated transport over the relevant range of operating condition. Experimental validation follows a defined hierarchy, progressing from simplified electrolytes to representative real feeds, with standardized reporting of membrane geometry, solution composition, driving force, ion-specific flux, selectivity, temporal stability, complete mass balances and the energy consumption per kilogram of target ion recovered. Time-resolved flux and mass-balance data must, in addition, be used to distinguish genuine membrane mass-transport effects from transient adsorption and ion-exchange contributions, because batch uptake or exchanger-like retention can masquerade as steady-state permselectivity in short-duration experiments. Collectively, these advances move the field away from phenomenological structure–performance correlations and toward mechanistically grounded, quantitatively predictive design principles. The resulting framework furnishes a rigorous basis for engineering ion-selective two-dimensional membranes with reproducible performance across solution conditions and operating periods. Translating lab-scale 2D membrane ion-separation technologies into practical seawater- and brine-recovery applications still faces multiple interconnected bottlenecks. Priority research directions include: (1) robust wet-state structural stabilization under real high-salinity feeds; (2) quantitative decoupling of multiple coexisting transport mechanisms; (3) systematic evaluation of long-term stability, fouling resistance, and membrane regeneration performance; (4) unified standardised report-

ing frameworks for separation metrics and mass balance. Progress on these fronts will bridge the gap between promising laboratory-scale selectivity results and industrially viable resource-recovery workflows.

Author Contributions: Conceptualization, W.Z., Y.Y. and N.L.; methodology, W.Z. and Y.Y.; software, W.Z.; validation, W.Z., Y.Y., N.L., Z.W. and J.R.; formal analysis, W.Z. and Y.Y.; investigation, W.Z. and Y.Y.; resources, N.L.; data curation, W.Z.; writing—original draft preparation, W.Z. and Y.Y.; writing—review and editing, N.L., Z.W. and J.R.; visualization, W.Z. and Y.Y.; supervision, N.L.; project administration, N.L.; funding acquisition, W.Z. All authors have read and agreed to the published version of the manuscript.

Funding: This research was funded by the National Natural Science Foundation of China (No. 52100011) and Tianjin Natural Science Foundation (No. 25JCYBJC00080).

Data Availability Statement: No new data were created or analyzed in this study. Data sharing is not applicable to this article.

Conflicts of Interest: Author Zhiwei Wang was employed by the company Tianjin Municipal Engineering Design & Research Institute Co., Ltd. Author Jianran Ren was employed by the company China Southwest Architecture Design and Research Institute Co., Ltd. The remaining authors declare that the research was conducted in the absence of any commercial or financial relationships that could be construed as a potential conflict of interest.

References

1. Yang, S.; Wang, Y.; Pan, H.; He, P.; Zhou, H. Lithium extraction from low-quality brines. *Nature* **2024**, *636*, 309–321. [CrossRef] [PubMed]
2. Sharkh, B.A.; Al-Amoudi, A.A.; Farooque, M.; Fellows, C.M.; Ihm, S.; Lee, S.; Li, S.; Voutchkov, N. Seawater desalination concentrate—A new frontier for sustainable mining of valuable minerals. *npj Clean Water* **2022**, *5*, 9. [CrossRef]
3. Zhang, X.; Zhao, W.; Zhang, Y.; Jegatheesan, V. A review of resource recovery from seawater desalination brine. *Rev. Environ. Sci. Bio/Technol.* **2021**, *20*, 333–361. [CrossRef]
4. Loganathan, P.; Naidu, G.; Vigneswaran, S. Mining valuable minerals from seawater: A critical review. *Environ. Sci. Water Res. Technol.* **2017**, *3*, 37–53. [CrossRef]
5. Guidez, J.; Gabriel, S. Extraction of uranium from seawater: A few facts. *EPJ Nucl. Sci. Technol.* **2016**, *2*, 10. [CrossRef]
6. Tachibana, Y.; Kalak, T.; Tanaka, M. Chromatographic Purification of Lithium, Vanadium, and Uranium from Seawater Using Organic Composite Adsorbents Composed of Benzo-18-Crown-6 and Benzo-15-Crown-5 Embedded in Highly Porous Silica Beads. *ACS Omega* **2022**, *7*, 27410–27421. [CrossRef] [PubMed]
7. Nikkhah, H.; Ipekçi, D.; Xiang, W.; Stoll, Z.; Xu, P.; Li, B.; McCutcheon, J.R.; Beykal, B. Challenges and opportunities of recovering lithium from seawater, produced water, geothermal brines, and salt lakes using conventional and emerging technologies. *Chem. Eng. J.* **2024**, *498*, 155349. [CrossRef]
8. Zhao, Y.; Mamrol, N.; Tarpeh, W.A.; Yang, X.; Gao, C.; Van der Bruggen, B. Advanced ion transfer materials in electro-driven membrane processes for sustainable ion-resource extraction and recovery. *Prog. Mater. Sci.* **2022**, *128*, 100958. [CrossRef]
9. Gaber, R.I.; Hong, S.; Abdulhamid, M.A.; Bahamon, D.; Vega, L.F.; Alhseinat, E. Ion-selective membranes: Highly efficient, robust, and superiorly selective. *J. Membr. Sci.* **2025**, 124890. [CrossRef]
10. Li, L.; Liu, B.; Li, Z. Metal–organic framework-based membranes for ion separation/selection from salt lake brines and seawater. *Nanoscale* **2024**, *16*, 19543–19563. [CrossRef] [PubMed]
11. Razmjou, A.; Asadnia, M.; Hosseini, E.; Habibnejad Korayem, A.; Chen, V. Design principles of ion selective nanostructured membranes for the extraction of lithium ions. *Nat. Commun.* **2019**, *10*, 5793. [CrossRef] [PubMed]
12. Huang, Q.; Kan, M.; Wang, S.; Shen, C.; Zhao, F.; Wang, L.; Li, D.; Liu, X.; Xu, L.; Dong, L.; et al. Graphene oxide based membranes for selective ion/molecule transport in water. *Adv. Colloid Interface Sci.* **2026**, *350*, 103772. [CrossRef] [PubMed]
13. Yuan, G.; Fang, J.; Sun, Y.; Ma, J.; Wang, H.; Zhou, W.; Jiang, Y.; Yang, C.; Zhou, Z.; Hu, R. Chemically gated ion transport in two-dimensional heterogeneous membranes with ultrahigh metal ion selectivity. *Sci. Bull.* **2025**, *70*, 3183–3189. [CrossRef] [PubMed]
14. Luo, J.; Qiao, R.; Ding, B. Enhancement of ion selectivity and permeability in two-dimensional material membranes. *Matter* **2024**, *7*, 3351–3389. [CrossRef]

15. Yang, R.; Liang, Z.; Wu, B.; Di, Y.; Lin, Y.; Wu, S.; Liu, Q.; Liang, S. "Cation-Recognition" Effect of 2D Nanochannels in Graphene Oxide Membranes Intercalated with Ionic Liquid for High Desalination Performance. *Small* **2025**, *21*, 2406550. [CrossRef] [PubMed]
16. Chen, L.; Shi, G.; Shen, J.; Peng, B.; Zhang, B.; Wang, Y.; Bian, F.; Wang, J.; Li, D.; Qian, Z.; et al. Ion sieving in graphene oxide membranes via cationic control of interlayer spacing. *Nature* **2017**, *550*, 380–383. [CrossRef] [PubMed]
17. Zheng, S.; Tu, Q.; Urban, J.J.; Li, S.; Mi, B. Swelling of Graphene Oxide Membranes in Aqueous Solution: Characterization of Interlayer Spacing and Insight into Water Transport Mechanisms. *ACS Nano* **2017**, *11*, 6440–6450. [CrossRef] [PubMed]
18. Abraham, J.; Vasu, K.S.; Williams, C.D.; Gopinadhan, K.; Su, Y.; Cherian, C.T.; Dix, J.; Prestat, E.; Haigh, S.J.; Grigorieva, I.V.; et al. Tunable sieving of ions using graphene oxide membranes. *Nat. Nanotechnol.* **2017**, *12*, 546–550. [CrossRef] [PubMed]
19. Ma, X.; Zhu, X.; Wang, T.; Si, T.; Fan, J. Unveiling the importance of surface ionization on desalination and ion-sieving performance of graphene oxide membranes. *Sep. Purif. Technol.* **2024**, *341*, 126930. [CrossRef]
20. Xu, R.; Kang, Y.; Zhang, W.; Pan, B.; Zhang, X. Two-dimensional MXene membranes with biomimetic sub-nanochannels for enhanced cation sieving. *Nat. Commun.* **2023**, *14*, 4907. [CrossRef] [PubMed]
21. Liang, C.-J.; Le, T.-H.; Ham, Y.; Mantha, B.R.K.; Cheng, M.H.; Lin, J.J. Ethics of artificial intelligence and robotics in the architecture, engineering, and construction industry. *Autom. Constr.* **2024**, *162*, 105369. [CrossRef]
22. Zhao, K.; Lee, W.-C.; Rezaei, M.; Chi, H.-Y.; Li, S.; Villalobos, L.F.; Hsu, K.-J.; Zhang, Y.; Wang, F.-C.; Agrawal, K.V. Tuning Pore Size in Graphene in the Angstrom Regime for Highly Selective Ion–Ion Separation. *ACS Nano* **2024**, *18*, 5571–5580. [CrossRef] [PubMed]
23. Persson, I. Structure and size of complete hydration shells of metal ions and inorganic anions in aqueous solution. *Dalton Trans.* **2024**, *53*, 15517–15538. [CrossRef] [PubMed]
24. Ershov, A.; Xu, H.; Li, Y.; Tong, T.; Epsztein, R. Role of Ion Dehydration in Ion–Ion Selectivity of Dense Membranes. *Environ. Sci. Technol.* **2025**, *59*, 17997–18009. [CrossRef] [PubMed]
25. Wang, J.; Zhou, H.; Li, S.; Wang, L. Selective Ion Transport in Two-Dimensional Lamellar Nanochannel Membranes. *Angew. Chem. Int. Ed.* **2023**, *62*, e202218321. [CrossRef] [PubMed]
26. Beccia, M.R.; Matara-Aho, M.; Reeves, B.; Roques, J.; Solari, P.L.; Monfort, M.; Moulin, C.; Den Auwer, C. New insight into the ternary complexes of uranyl carbonate in seawater. *J. Environ. Radioact.* **2017**, *178–179*, 343–348. [CrossRef] [PubMed]
27. Kim, G.W.; Lee, M.; Bae, J.; Han, J.; Park, S.; Shim, W. Li-ion transport in two-dimensional nanofluidic membranes. *Nano Converg.* **2024**, *11*, 54. [CrossRef] [PubMed]
28. Liao, S.; Liu, Y.; Li, L.; Ding, L.; Wei, Y.; Wang, H. Theoretical framework for confined ion transport in two-dimensional nanochannels. *Nat. Commun.* **2025**, *16*, 6675. [CrossRef] [PubMed]
29. Joshi, R.; Carbone, P.; Wang, F.-C.; Kravets, V.G.; Su, Y.; Grigorieva, I.V.; Wu, H.; Geim, A.K.; Nair, R.R. Precise and ultrafast molecular sieving through graphene oxide membranes. *Science* **2014**, *343*, 752–754. [CrossRef] [PubMed]
30. Zhao, W.; Yin, P.; Wang, Z.; Huang, J.; Fu, Y.; Hu, W. Recent advances in regulation methods for selective separation and precise control of two-dimensional (2D) lamellar membranes. *Adv. Colloid Interface Sci.* **2024**, *334*, 103330. [CrossRef] [PubMed]
31. Zhang, T.; Ren, B.; Bai, H.; Wen, T.; Chen, L.; Ma, S.; Wang, X.; Wang, S.; Zhao, Y. Subnanometer-scale control of channel height in two-dimensional montmorillonite membrane for ion separation. *J. Membr. Sci.* **2023**, *675*, 121573. [CrossRef]
32. Wang, J.; Wang, A.; Liu, J.; Niu, Q.; Zhang, Y.; Liu, P.; Liu, C.; Wang, H.; Zeng, X.; Zeng, G. Polyethyleneimine modified two-dimensional GO/MXene composite membranes with enhanced Mg2+/Li+ separation performance for salt Lake brine. *Molecules* **2024**, *29*, 4326. [CrossRef] [PubMed]
33. Wu, Y.; Jia, M.; Li, S.; Lu, Z.; Wei, Y.; Wang, H. Positively charged $Ti_3C_2T_x$ membrane for enhanced Li+/Mg2+ sieving. *J. Membr. Sci.* **2025**, *717*, 123604. [CrossRef]
34. Zhang, M.; Guan, K.; Ji, Y.; Liu, G.; Jin, W.; Xu, N. Controllable ion transport by surface-charged graphene oxide membrane. *Nat. Commun.* **2019**, *10*, 1253. [CrossRef] [PubMed]
35. Zhao, B.; Liu, H.; Hao, Y.; Zhao, M.; Zhou, K.-G. Emerging Selective Ion Transport via 2D Confined Space for the Innovations in Separation and Energy Technologies. *ACS Appl. Mater. Interfaces* **2025**, *17*, 55751–55780. [CrossRef] [PubMed]
36. Mo, R.-J.; Chen, S.; Huang, L.-Q.; Ding, X.-L.; Rafique, S.; Xia, X.-H.; Li, Z.-Q. Regulating ion affinity and dehydration of metal-organic framework sub-nanochannels for high-precision ion separation. *Nat. Commun.* **2024**, *15*, 2145. [CrossRef] [PubMed]
37. Wang, M.; Xiong, Q.; Yue, X.; Yan, G.; Han, Y.; Lyu, Z.; Li, Z.; Sun, L.; Hoenig, E.; Xu, K.; et al. Cooperative and inhibitory ion transport in functionalized angstrom-scale two-dimensional channels. *Nat. Commun.* **2025**, *16*, 5854. [CrossRef] [PubMed]
38. Zhou, X.; Zhang, Y.; Chen, Z.; Zhao, S.; Yang, H.; Liu, G.; Ji, W.; Guo, Y.; Liu, G.; Jin, W. Crown Ether Confined in a 2D MXene Membrane for Mono-/Divalent Ion Separation. *Ind. Eng. Chem. Res.* **2025**, *64*, 17844–17852. [CrossRef]
39. Yuan, Y.; Cao, D.; Cui, F.; Yang, Y.; Zhang, C.; Song, Y.; Zheng, Y.; Cao, J.; Chen, S.; Song, Y.; et al. High-capacity uranium extraction from seawater through constructing synergistic multiple dynamic bonds. *Nat. Water* **2025**, *3*, 89–98. [CrossRef]
40. Smolyanitsky, A.; Fang, A.; Kazakov, A.F.; Paulechka, E. Ion transport across solid-state ion channels perturbed by directed strain. *Nanoscale* **2020**, *12*, 10328–10334. [CrossRef] [PubMed]

41. Zhang, Z.; Bhauriyal, P.; Sahabudeen, H.; Wang, Z.; Liu, X.; Hambsch, M.; Mannsfeld, S.C.B.; Dong, R.; Heine, T.; Feng, X. Cation-selective two-dimensional polyimine membranes for high-performance osmotic energy conversion. *Nat. Commun.* **2022**, *13*, 3935. [CrossRef] [PubMed]
42. Bao, S.; Ma, Z.; Yu, L.; Li, Q.; Xia, J.; Song, S.; Sui, K.; Zhao, Y.; Liu, X.; Gao, J. Randomly oriented covalent organic framework membrane for selective Li+ sieving from other ions. *Nat. Commun.* **2025**, *16*, 3896. [CrossRef] [PubMed]
43. Meng, Q.-W.; Li, J.; Xing, Z.; Xian, W.; Lai, Z.; Dai, Z.; Wang, S.; Zhang, L.; Yin, H.; Ma, S.; et al. Regulation of Ion Binding Sites in Covalent Organic Framework Membranes for Enhanced Selectivity under High Ionic Competition. *ACS Nano* **2025**, *19*, 12080–12089. [CrossRef] [PubMed]
44. Sun, Q.; Dou, P.; Du, J.; Yao, A.; Cao, D.; Ma, J.; Hassan, S.U.; Guan, J.; Liu, J. Biomimetic KcsA channels enabled by 1D MOF-in-2D COF. *Nat. Commun.* **2025**, *16*, 9099. [CrossRef] [PubMed]
45. Rollings, R.C.; Kuan, A.T.; Golovchenko, J.A. Ion selectivity of graphene nanopores. *Nat. Commun.* **2016**, *7*, 11408. [CrossRef] [PubMed]
46. Sahu, S.; Di Ventra, M.; Zwolak, M. Dehydration as a Universal Mechanism for Ion Selectivity in Graphene and Other Atomically Thin Pores. *Nano Lett.* **2017**, *17*, 4719–4724. [CrossRef] [PubMed]
47. Sahu, S.; Zwolak, M. Ionic selectivity and filtration from fragmented dehydration in multilayer graphene nanopores. *Nanoscale* **2017**, *9*, 11424. [CrossRef] [PubMed]
48. Fu, Y.; Su, S.; Zhang, N.; Wang, Y.; Guo, X.; Xue, J. Dehydration-Determined Ion Selectivity of Graphene Subnanopores. *ACS Appl. Mater. Interfaces* **2020**, *12*, 24281–24288. [CrossRef] [PubMed]
49. Zhao, N.; Deng, J.; Zhu, Y.; Chen, Y.; Qin, Y.; Ruan, Y.; Zhang, Y.; Gao, Q.; Lu, X. Atomistic insights into the effects of carbonyl oxygens in functionalized graphene nanopores on Ca^{2+}/Na^{+} sieving. *Carbon* **2020**, *164*, 305–316. [CrossRef]
50. Zhu, Y.; Xiong, Q.; Jeon, W.C.; Blum, M.; Camino, F.; Schatz, G.C.; Hatzell, K.B. Water content modulation enables selective ion transport in 2D MXene membranes. *Proc. Natl. Acad. Sci. USA* **2025**, *122*, e2501017122. [CrossRef] [PubMed]
51. Wang, Z.; Huang, L.; Dong, X.; Wu, T.; Qing, Q.; Chen, J.; Lu, Y.; Xu, C. Ion sieving in graphene oxide membrane enables efficient actinides/lanthanides separation. *Nat. Commun.* **2023**, *14*, 261. [CrossRef] [PubMed]
52. Booth, A.J.; Xiong, Q.; Jeon, W.C.; Schatz, G.C.; Hatzell, K.B. Coordinated Cation Transport in $Ti_3C_2T_x$ MXene Membranes. *ACS Appl. Mater. Interfaces* **2025**, *17*, 38062–38072. [CrossRef] [PubMed]
53. Bucs, S.; Jung, O.; Wagner, M.; Saravia, F.; Horn, H.; Picioreanu, C. Raman micro-spectroscopy for the study of concentration polarization in the presence of biofouling in pressure driven membrane systems. *J. Membr. Sci.* **2025**, *713*, 123219. [CrossRef]
54. Li, W.; Wu, W.; Li, Z. Controlling Interlayer Spacing of Graphene Oxide Membranes by External Pressure Regulation. *ACS Nano* **2018**, *12*, 9309–9317. [CrossRef] [PubMed]
55. Wang, Z.; Ma, C.; Xu, C.; Sinquefield, S.A.; Shofner, M.L.; Nair, S. Graphene oxide nanofiltration membranes for desalination under realistic conditions. *Nat. Sustain.* **2021**, *4*, 402–408. [CrossRef]
56. Lu, Z.; Wu, Y.; Ding, L.; Wei, Y.; Wang, H. A Lamellar MXene ($Ti_3C_2T_x$)/PSS Composite Membrane for Fast and Selective Lithium-Ion Separation. *Angew. Chem. Int. Ed.* **2021**, *60*, 22265–22269. [CrossRef] [PubMed]
57. Meng, Q.-W.; Zhu, X.; Xian, W.; Wang, S.; Zhang, Z.; Zheng, L.; Dai, Z.; Yin, H.; Ma, S.; Sun, Q. Enhancing ion selectivity by tuning solvation abilities of covalent-organic-framework membranes. *Proc. Natl. Acad. Sci. USA* **2024**, *121*, e2316716121. [CrossRef] [PubMed]
58. Ye, T.; Gao, H.; Li, Q.; Liu, N.; Liu, X.; Jiang, L.; Gao, J. Highly Selective Lithium Transport through Crown Ether Pillared Angstrom Channels. *Angew. Chem. Int. Ed.* **2024**, *63*, e202316161. [CrossRef] [PubMed]
59. Dong, X.; Ai, X.; He, W.; Zhai, Y.; Guo, R.; Li, Y.-W.; Ma, Z.-Q.; Yang, Y.; Zhou, K.-G. Heteropolyacid Ligands in Two-Dimensional Channels Enable Lithium Separation from Monovalent Cations. *ACS Nano* **2025**, *19*, 4233–4241. [CrossRef] [PubMed]
60. Dai, L.; Guan, K.; Mai, Z.; Fang, S.; Zhao, S.; Hu, M.; Li, Z.; Zhang, P.; Xu, P.; Matsuyama, H. Sodium-Ion Traps in a Two-Dimensional Confined Channel for Effective Water and Ion Selective Transport. *Nano Lett.* **2024**, *24*, 13686–13694. [CrossRef] [PubMed]
61. Zhou, Z.; Zhao, K.; Chi, H.-Y.; Shen, Y.; Song, S.; Hsu, K.-J.; Chevalier, M.; Shi, W.; Agrawal, K.V. Electrochemical-repaired porous graphene membranes for precise ion-ion separation. *Nat. Commun.* **2024**, *15*, 4006. [CrossRef] [PubMed]
62. Yuan, F.; Gao, Q.; Lv, Z.; Zhang, Y.; Liu, X.; Peng, J.; Li, Z. 2D Membranes Interlayered with Bimetallic Metal–Organic Frameworks for Lithium Separation from Brines. *Nano Lett.* **2024**, *24*, 14346–14354. [CrossRef] [PubMed]
63. Liu, L.; Huang, J.a.; Wang, Y.; Pang, D.; Ding, Y.; Liu, J.; Zhang, X.; Guo, C.; Jia, J.; Zhang, M.; et al. Engineering Crystalline Frameworks into Porous Liquids to Fabricate Graphene Oxide/Porous Liquid Membranes for Efficient Li+/Mg2+ Separation. *Nat. Commun.* **2026**, *17*, 7575. [CrossRef] [PubMed]
64. Wu, T.; Wang, Z.; Lu, Y.; Liu, S.; Li, H.; Ye, G.; Chen, J. Graphene Oxide Membranes for Tunable Ion Sieving in Acidic Radioactive Waste. *Adv. Sci.* **2021**, *8*, 2002717. [CrossRef] [PubMed]

65. Zhang, P.; Zhang, Y.; Wang, L.; Qiu, K.; Tang, X.; Gibson, J.K.; Liu, X.; Mei, L.; An, S.; Huang, Z.; et al. Bioinspired Macrocyclic Molecule Supported Two-Dimensional Lamellar Membrane with Robust Interlayer Structure for High-Efficiency Nanofiltration. *Adv. Sci.* **2022**, *10*, e2206516. [CrossRef] [PubMed]
66. Liu, T.; Li, Z.; Zhang, X.; Tan, H.; Chen, Z.; Wu, J.; Chen, J.; Qiu, H. Metal–Organic Framework-Intercalated Graphene Oxide Membranes for Selective Separation of Uranium. *Anal. Chem.* **2021**, *93*, 16175–16183. [CrossRef] [PubMed]
67. Liang, W.; Zhang, X.; Wang, L.; Wen, C.; Tian, L.; Li, Z.; Chen, X.; Wu, W. Designing biomimetic two-dimensional channels for uranium separation from seawater. *Chem. Sci.* **2024**, *15*, 10455–10463. [CrossRef] [PubMed]
68. Lv, Z.; Li, H.; Wen, C.; Tian, L.; Chen, X.; Wu, W.; Li, Z. 2D Biomimetic Membranes Constructed by Charge Assembly and Hydrogen Bonding for Precise Ion Separation. *Adv. Mater.* **2025**, *37*, 2419496. [CrossRef] [PubMed]
69. Tang, X.-Y.; Li, Z.-J.; Wang, L.; Zhang, P.-C.; Hu, K.-Q.; Zheng, L.-R.; Zhang, Z.-H.; Yuan, L.-Y.; Wu, W.-S.; Shi, W.-Q. Fabrication of graphene oxide/ammonium molybdophosphate composite membrane for decontamination of cesium ions from seawater. *Chem. Eng. J.* **2024**, *499*, 155974. [CrossRef]
70. Huang, Y.; Chen, J.; Liu, H.; Wang, Y.; Lu, M.; Liu, X.; Ye, X.; Shi, G. Crown ether intercalated graphene oxide membranes for highly efficient sieving of cesium with a large water permeability. *Sep. Purif. Technol.* **2024**, *339*, 126702. [CrossRef]
71. Fan, Q.; E, Z.; Shi, L.; Lu, Z.; Li, P.; Liang, J. Non-swelling oxidized graphene ribbon membrane for the effective separation of cesium and strontium from radioactive liquid waste. *J. Membr. Sci.* **2023**, *680*, 121727. [CrossRef]
72. Tan, Y.; Zhang, Y.L.; Ren, H.; Feng, S.; Xie, R.; Ju, X.J.; Wang, W.; Pan, D.W.; Deng, Y.C.; Zhou, X.L.; et al. Programming Ion Transport in Layered 2D Hybrid Membranes via Coordination-Occupation Coupling. *Adv. Mater.* **2026**, *38*, e73120. [CrossRef] [PubMed]
73. Wang, S.; Liang, S. Acid response nanochannels of graphene oxide membranes for fast nuclide ions separation. *Sep. Purif. Technol.* **2024**, *328*, 125086. [CrossRef]
74. Wei, Y.; Cao, L.; Zhu, J.; Wang, L.; Yao, H.; Sun, H.; Xia, X.; Zhao, H.; Ji, T.; Ni, S.; et al. Radioactive strontium ions sieving through reduced graphene oxide membrane. *J. Membr. Sci.* **2024**, *689*, 122181. [CrossRef]
75. Li, C.; Li, Z.; Guan, K.; Chiao, Y.-H.; Zhang, P.; Xu, P.; Gonzales, R.R.; Hu, M.; Mai, Z.; Yoshioka, T.; et al. Polyethylenimine-assisted preparation of Zr-MOF/GO membranes for radionuclide separation. *Desalination* **2024**, *592*, 118118. [CrossRef]
76. Vishwakarma, R.K.; Narayanam, P.K.; R, U.; K, S. Surface modified and functionalized graphene oxide membranes for separation of strontium from aqueous solutions. *J. Environ. Manag.* **2021**, *298*, 113443. [CrossRef] [PubMed]
77. Wang, H.; Zhai, Y.; Li, Y.; Cao, Y.; Shi, B.; Li, R.; Zhu, Z.; Jiang, H.; Guo, Z.; Wang, M.; et al. Covalent organic framework membranes for efficient separation of monovalent cations. *Nat. Commun.* **2022**, *13*, 7123. [CrossRef] [PubMed]
78. Lu, Y.; Wei, L.; Xie, Z.-a.; Wu, X.; Xue, H.; Su, H.; Liu, J.; Jing, M.; Chen, J.; Shi, G.; et al. Graphene oxide-polydopamine membranes with controlled interlayer spacing. *Nature* **2026**, *655*, 1180–1186. [CrossRef] [PubMed]
79. Sun, P.; Zhu, M.; Wang, K.; Zhong, M.; Wei, J.; Wu, D.; Xu, Z.; Zhu, H. Selective Ion Penetration of Graphene Oxide Membranes. *ACS Nano* **2012**, *7*, 428–437. [CrossRef] [PubMed]
80. Sun, P.; Zheng, F.; Zhu, M.; Song, Z.; Wang, K.; Zhong, M.; Wu, D.; Little, R.B.; Xu, Z.; Zhu, H. Selective Trans-Membrane Transport of Alkali and Alkaline Earth Cations through Graphene Oxide Membranes Based on Cation–π Interactions. *ACS Nano* **2014**, *8*, 850–859. [CrossRef] [PubMed]
81. Lu, Z.; Wei, Y.; Deng, J.; Ding, L.; Li, Z.-K.; Wang, H. Self-Crosslinked MXene ($Ti_3C_2T_x$) Membranes with Good Antiswelling Property for Monovalent Metal Ion Exclusion. *ACS Nano* **2019**, *13*, 10535–10544, Correction in *ACS Nano* **2023**, *17*, 12934. [CrossRef] [PubMed]
82. Ding, L.; Li, L.; Liu, Y.; Wu, Y.; Lu, Z.; Deng, J.; Wei, Y.; Caro, J.; Wang, H. Effective ion sieving with $Ti_3C_2T_x$ MXene membranes for production of drinking water from seawater. *Nat. Sustain.* **2020**, *3*, 296–302. [CrossRef]
83. Wang, J.; Zhang, Z.; Zhu, J.; Tian, M.; Zheng, S.; Wang, F.; Wang, X.; Wang, L. Ion sieving by a two-dimensional $Ti_3C_2T_x$ alginate lamellar membrane with stable interlayer spacing. *Nat. Commun.* **2020**, *11*, 3540. [CrossRef] [PubMed]
84. Ren, C.E.; Hatzell, K.B.; Alhabeb, M.; Ling, Z.; Mahmoud, K.A.; Gogotsi, Y. Charge- and Size-Selective Ion Sieving Through $Ti_3C_2T_x$ MXene Membranes. *J. Phys. Chem. Lett.* **2015**, *6*, 4026–4031. [CrossRef] [PubMed]
85. Kang, Y.; Hu, T.; Wang, Y.; He, K.; Wang, Z.; Hora, Y.; Zhao, W.; Xu, R.; Chen, Y.; Xie, Z.; et al. Nanoconfinement enabled non-covalently decorated MXene membranes for ion-sieving. *Nat. Commun.* **2023**, *14*, 4075. [CrossRef] [PubMed]
86. Xu, R.; Zhang, J.; Kang, Y.; Yu, H.; Zhang, W.; Hua, M.; Pan, B.; Zhang, X. Reversible pH-Gated MXene Membranes with Ultrahigh Mono-/Divalent-Ion Selectivity. *Environ. Sci. Technol.* **2024**, *58*, 6835–6842. [CrossRef] [PubMed]
87. Wang, X.; Zhang, H.; Wei, G.; Xing, J.; Chen, S.; Quan, X. Comediation of voltage gating and ion charge in MXene membrane for controllable and selective monovalent cation separation. *Sci. Adv.* **2024**, *10*, eado3998. [CrossRef] [PubMed]
88. Huang, L.; Chen, S.; Ding, L.; Wang, H. Lateral-Size-Dependent Ion Transport Behavior of the MXene Membrane Facilitates Efficient Ion Sieving. *ACS Appl. Nano Mater.* **2024**, *7*, 9482–9489. [CrossRef]
89. Hoenig, E.; Han, Y.; Xu, K.; Li, J.; Wang, M.; Liu, C. In situ generation of (sub) nanometer pores in MoS2 membranes for ion-selective transport. *Nat. Commun.* **2024**, *15*, 7911. [CrossRef] [PubMed]

90. Ries, L.; Petit, E.; Michel, T.; Diogo, C.C.; Gervais, C.; Salameh, C.; Bechelany, M.; Balme, S.; Miele, P.; Onofrio, N.; et al. Enhanced sieving from exfoliated MoS2 membranes via covalent functionalization. *Nat. Mater.* **2019**, *18*, 1112–1117. [CrossRef] [PubMed]
91. Shen, J.; Aljarb, A.; Cai, Y.; Liu, X.; Min, J.; Wang, Y.; Wang, Q.; Zhang, C.; Chen, C.; Hakami, M.; et al. Engineering grain boundaries in monolayer molybdenum disulfide for efficient water-ion separation. *Science* **2025**, *387*, 776–782. [CrossRef] [PubMed]
92. Cao, L.; Chen, I.C.; Li, Z.; Liu, X.; Mubashir, M.; Nuaimi, R.A.; Lai, Z. Switchable Na+ and K+ selectivity in an amino acid functionalized 2D covalent organic framework membrane. *Nat. Commun.* **2022**, *13*, 7894. [CrossRef] [PubMed]
93. Lv, Y.; Dai, Z.; Chen, Y.; Lu, Y.; Zhang, X.; Yu, J.; Zhai, W.; Yu, Y.; Wen, Z.; Cui, Y.; et al. Two-Dimensional Sulfonate-Functionalized Metal–Organic Framework Membranes for Efficient Lithium-Ion Sieving. *Nano Lett.* **2024**, *24*, 2782–2788. [CrossRef] [PubMed]
94. Zhang, T.; Bai, H.; Zhao, Y.; Ren, B.; Wen, T.; Chen, L.; Song, S.; Komarneni, S. Precise Cation Recognition in Two-Dimensional Nanofluidic Channels of Clay Membranes Imparted from Intrinsic Selectivity of Clays. *ACS Nano* **2022**, *16*, 4930–4939. [CrossRef] [PubMed]
95. Pang, S.; Dai, L.; Yi, Z.; Qu, K.; Wang, Y.; Wu, Y.; Fang, C.; Huang, K.; Xu, Z. 2D nanofluidic vermiculite membranes with self-confinement channels and recognition sites for ultrafast lithium ion-selective transport. *J. Membr. Sci.* **2023**, *687*, 122054. [CrossRef]
96. Liu, Y.; Wang, Y.; Sengupta, B.; Kazi, O.A.; Martinson, A.B.F.; Elam, J.W.; Darling, S.B. Pillared Laminar Vermiculite Membranes with Tunable Monovalent and Multivalent Ion Selectivity. *Adv. Mater.* **2025**, *37*, 2417994. [CrossRef] [PubMed]
97. Ma, Z.; Fan, J.; Zhu, C.; Gao, H.; Gao, J. Deep Dehydrated Layered Vermiculite Membrane for Selective Lithium Separation. *Angew. Chem. Int. Ed.* **2026**, *65*, e9661914. [CrossRef] [PubMed]
98. Hao, Y.; Liu, X.; Zhang, Y.; Zhang, X.; Li, Z.; Chen, X. Fine-Tuning 2D Heterogeneous Channels for Charge-Lock Enhanced Lithium Separation from Brine. *Adv. Sci.* **2024**, *11*, 2406535. [CrossRef] [PubMed]
99. Rahbari-Sisakht, M.; Ismail, A.F.; Goh, P.S.; Abdullah, M.S.; Raharjo, Y. Two-dimensional nanomaterials in membrane-based water purification: Advances, challenges, and future perspectives. *Desalination* **2026**, *625*, 119935. [CrossRef]
100. Ansari, A.; Peña-Bahamonde, J.; Wang, M.; Shaffer, D.L.; Hu, Y.; Rodrigues, D.F. Polyacrylic acid-brushes tethered to graphene oxide membrane coating for scaling and biofouling mitigation on reverse osmosis membranes. *J. Membr. Sci.* **2021**, *630*, 119308. [CrossRef]
101. Tandel, A.M.; Agarwal, M.; Deng, E.; Zhu, L.; Friedman, K.; Yu, M.; Cheng, C.; Lin, H. Scalable Graphene Oxide Hollow Fiber Membranes for Dye Desalination Enabled by Multi-Purpose Polyamine Functionalization. *Small* **2024**, *20*, 2403620. [CrossRef] [PubMed]
102. Liu, G.; Guo, Y.; Meng, B.; Wang, Z.; Liu, G.; Jin, W. Two-dimensional MXene hollow fiber membrane for divalent ions exclusion from water. *Chin. J. Chem. Eng.* **2022**, *41*, 260–266. [CrossRef]
103. Wei, Y.; Gao, X.; Wang, J.; Chen, J.; Mi, B.; Tian, X.; Gao, C.; Zhang, Y. Facile and extensible preparation of multi-layered graphene oxide membranes with enhanced long-term desalting performance. *J. Membr. Sci.* **2021**, *638*, 119695. [CrossRef]
104. Kang, Y.; Xia, Y.; Wang, H.; Zhang, X. 2D Laminar Membranes for Selective Water and Ion Transport. *Adv. Funct. Mater.* **2019**, *29*, 1902014. [CrossRef]
105. DuChanois, R.M.; Porter, C.J.; Violet, C.; Verduzco, R.; Elimelech, M. Membrane Materials for Selective Ion Separations at the Water–Energy Nexus. *Adv. Mater.* **2021**, *33*, 2101312. [CrossRef] [PubMed]
106. Wang, R.; Lin, S. Membrane Design Principles for Ion-Selective Electrodialysis: An Analysis for Li/Mg Separation. *Environ. Sci. Technol.* **2024**, *58*, 3552–3563. [CrossRef] [PubMed]

Disclaimer/Publisher's Note: The statements, opinions and data contained in all publications are solely those of the individual author(s) and contributor(s) and not of MDPI and/or the editor(s). MDPI and/or the editor(s) disclaim responsibility for any injury to people or property resulting from any ideas, methods, instructions or products referred to in the content.